CHAVEZ, JESSICA, M.S. Carbon Nanodot Cellular Uptake and Modulation of Tumor Necrosis Factor-Alpha-Induced Endothelial Dysfunction. (2018).
Directed by Dr. Zhenquan Jia. 57pp.

In the past forty years, we have advanced our understanding of cardiovascular pathology through epidemiological and molecular studies. Atherosclerosis is one of the main cardiovascular diseases, which is also an underlying cause of more severe cardiovascular pathologies. Atherosclerosis is the chronic inflammatory response initiated by the damage to the endothelium caused by an imbalance of reactive oxygen species (ROS). This chronic inflammation causes the accumulation of plaque in arterial walls. Due to the widespread of cardiovascular disease, finding better treatment options is of importance. The interdisciplinary field of nanomedicine has been studying the application of various nanoparticles for future treatment options. A new class of nanoparticles that has promising features for medical application is carbon nanodots (CND). The citric acid-ethylenediamine synthesized CNDs used in this study have antioxidant properties making them candidates for quenching ROS and decreasing cardiovascular inflammation. Previous studies have shown that carbon nanodots have low toxicity in numerous cell lines, but CND exposure to endothelial cells has not been explored. The main goal of this study is to analyze *in vitro* and *in vivo* the effect of CNDs on endothelial dysfunction.

Our *in vitro* results showed that the uptake of carbon nanodots by EA.hy926 endothelial cells is both time and dose-dependent. Our experiments showed cell-viability

consistent with previous studies showing that nanodots have low cytotoxicity after 24 hr exposure with lower CND concentrations up to 0.3 mg/mL. However, we also found that higher concentrations affect metabolic activity via MTT assay after 6 hr exposure. CNDs significantly inhibited TNF-α-mediated expression of intracellular adhesion molecule-1 (ICAM-1), and interleukin 8, two key molecules that are responsible for the activation and the firm adhesion of monocytes to activated endothelial cells for the initiation of atherosclerosis, while the mRNA levels increased for monocyte chemoattractant protein-1 (MCP-1/CCL2). Similarly to the previously mentioned results, the gene expression of pro-inflammatory genes in cells that were treated with carbon nanodots alone showed a change in gene expression. Additional data showed that NQO1 activity is increased by nanodots after 24 hr treatment, this phase II cytoprotective enzyme is known to maintain homeostasis in the vasculature. Histology of samples from our 8-week animal study in apolipoprotein E knockout mice (Apo E -/-) suggest that plaque formation in the aorta is decreased in animals dosed with CNDs. Tissue samples from the liver of mice dosed with CNDs appear to have a decrease in hepatic lipidosis, while the kidney which is also an important detoxifying organ seems to have no significant change in histology.

In conclusion, this study explored the bioapplication of carbon nanodots in endothelial cell dysfunction, and our results showed that carbon nanodots could be promising nanoparticles that may decrease cardiovascular inflammation. Future studies need to explore the role of the NF-κB pathway and the Nrf2 pathway activation to understand the underlying mode of action by which pro-inflammatory gene expression changes, and NQO1 enzymatic activity increases.

CARBON NANODOT CELLULAR UPTAKE AND MODULATION OF TUMOR NECROSIS FACTOR-ALPHA-INDUCED ENDOTHELIAL DYSFUNCTION

by

Jessica Chavez

A Thesis Submitted to
the Faculty of The Graduate School at
The University of North Carolina at Greensboro
in Partial Fulfillment
of the Requirements for the Degree
Master of Science

Greensboro
2018

Approved by

_____
Committee Chair

Este tesis está dedicado a mi familia. Especialmente a mi madre Gudelia y mi papá Miguel, quienes me han apoyado a lo largo de este camino, y a mi abuelo Tomás. This work is also dedicated to my sisters, thank you for pretending to know what I was talking about when I explained my research. Thank you to all the mentors I have had along the way especially my ESL teacher Mrs. Cheryl White, and my undergraduate advisor Dr. Kelli Sapp for opening my interests in the field of biology.

APPROVAL PAGE

This thesis written by Jessica Chavez has been approved by the following committee of the Faculty of The Graduate School at The University of North Carolina at Greensboro.

Committee Chair _____
Zhenquan Jia

Committee Members _____
Yashomati Patel

_____
Jianjun Wei

_____
Date of Acceptance by Committee

_____
Date of Final Oral Examination

ACKNOWLEGEMENTS

I would like to thank my advisor Dr. Zhenquan Jia for giving me the opportunity to grow as a scientist in his research lab, and my committee members Dr. Yashomati Patel and Dr. Jianjun Wei; thank you for your guidance and support. I would like to thank my lab members especially Ho Young Lee, Halley Shah, and Safeera Khan for their assistance along this journey. My gratitude goes to Jonah Nikouyeh, Steven Moran, and Dana Jeffus for their constant encouragement and support. I would also like to thank our collaborators at JSNN, and Michigan State Medical School. A big thank you to biology department and the NIH for their help in funding this research.

TABLE OF CONTENTS

Page

LIST OF TABLES

Page

LIST OF FIGURES

Page

CHAPTER I

INTRODUCTION

Cardiovascular Disease

Chronic diseases are amongst the leading cause of death and disability in the United States, the chronic disease that tops the list is cardiovascular disease (CVD). According to the 2014 U.S. mortality data, heart disease had the highest death rate for both sexes as well as across ethnicities. Currently, heart disease remains the main cause of death in the United States [1, 2]. The American Heart Association predicted that by 2030 40% of the U.S. population would suffer from a form of cardiovascular disease, but, by 2015 41.5% of the American population had a form of CVD [3]. Atherosclerosis, the buildup of plaque (e.g., fat, cholesterol, etc.) inside arteries, is a precursor to more severe cardiovascular diseases. It is a multi-factorial disease that can be influenced by genetic, behavioral health, and environmental factors that mainly affect the heart. The hardening of coronary arteries is the underlying cause of multiple chronic heart health issues. The silent progression of atherosclerosis can lead to ischemic damage that can cause myocardial infarction events, ensuing the placement of drug eluding stents via percutaneous coronary intervention. This cardiac event would be followed by a regimen of high-risk medications needed to prevent a future cardiac event. By the year 2035, it is estimated that the cost of cardiovascular diseases will surpass the $1 trillion mark, making it not only a health concern but also an economic burden [3, 4]. CVDs account

for about 31% of worldwide deaths [5], making it of worldwide health importance to search for potential preventative measures and treatments to limit the growing burden.

The Role of Inflammation in the Initiation of Atherosclerosis

The pathogenesis of the atherosclerotic vascular disease is a complex process, but accumulating data shows that inflammation is an important protagonist in subsequent atypical endothelial cell functions (i.e., endothelial dysfunction), playing a fundamental role in the initiation and progression of atherosclerosis. In a healthy artery, endothelial cells line the internal lumen of the vasculature, and they are lined by the tunica intima. The hardening of the arteries occurs when endothelial cells are activated, and pro-inflammatory mediators coordinate leukocyte migration and extravasion of leukocytes into the tunica intima, the site of endothelial activation. The continuous migration of white blood cells causes the thickening of the artery cell wall, leading to various health complications as the diameter of the artery is narrowed, and blood flow decreases [6]. The mediators that signal for inflammation are cytokines and adhesion molecules. Pro-inflammatory mediators are secreted molecules which include thrombin, tumor necrosis factor-alpha (TNF-α), macrophage chemoattractant protein-1 (MCP-1 also known as CCL2), interleukin 8 (IL-8), E-selectin, P-selectin, vascular cell adhesion molecule-1 (VCAM-1), and intracellular adhesion molecule-1 (ICAM-1) [7-10]. Studies show that TNFα is an important pro-inflammatory mediator. Currently, there is not an effective treatment that can decrease the expression of cytokines. Inflammation-induced endothelial dysfunction is important in the development of atherosclerosis, and agents

that can suppress the inflammatory pathway in vascular endothelial cells are candidate agents to prevent or treat vascular endothelial dysfunction.

Atherosclerosis is an inflammatory disease, and it is the precursor to multiple cardiovascular diseases. In the presence of an atherosclerotic lesion, alterations occur within the endothelial cells, resulting in transcriptional activation of inflammatory genes through the activation of the nuclear factor kappa B (NF-κB) pathway [11-13]. Endothelial cells are one of the few cells not part of the immune system that can excrete messenger molecules to attract leukocytes to the site of inflammation. Activated (or dysfunctional) endothelium can also express adhesion molecules, facilitating the adhesion of white blood cells to the site of inflammation. The inflammatory response commences when leukocytes have successfully attached to the damaged endothelium, and transmigrate into the intima region. Leukocytes, mainly monocytes, are activated into macrophages once they have migrated into the intima. In the intima, the macrophages can phagocytize oxidized lipids, such as lipoproteins. Through lipid accumulation, these macrophages turn into “foam cells” which accumulate through continuous inflammation to create fatty streaks [14]. Macrophages consequently undergo apoptosis, and signal for reinforcement by secreting cytokines, which recruit more leukocytes. Eventually, the vessel matrix will form finalize the formation of plaque. It has also been documented that local sheer stress can promote the expression of adhesion molecules, augmenting the inflammatory response and impacting atherosclerosis development [15, 16]. In a healthy vessel, the blood flow typically helps regulate genes that are relevant to atherogenesis.

Reactive Oxygen Species and Atherosclerosis

One of the main sources of cellular damage is oxidative stress. Cellular oxidative stress occurs when the production of reactive oxygen species surpasses the capability of the enzymatic antioxidants to regulate the levels of reactive oxygen species (ROS). ROS are derived byproducts from elemental oxygen, which can regulate cell functions. Low levels of ROS can help regulate cell functions, whereas high concentrations can alter macromolecules. Inadequate ROS balance can alter vascular homeostasis by inactivating nitric oxide (NO), which defends against vascular disease development [6, 17]. Nitric oxide, a vaso-protector, is a major target of superoxide. When superoxide reacts with NO, peroxynitrite (vasotoxic) is formed, which in return oxidizes BH_4, a co-factor of eNOS, the enzyme responsible for producing NO [18]. Cells generate ROS in the vascular wall, in the mitochondria through oxidative phosphorylation, which can cause damage to lipids, proteins, and even mitochondrial DNA [19]. In response to a high concentration of ROS, antioxidant enzymes are induced to protect against not only reactive oxygen species, but other types of free radicals by scavenging the reactive molecules preventing the damage macromolecules. The imbalance between reactive oxygen species and antioxidant enzymes is a critical event in endothelial activation [20]. Endothelial activation refers to the state of endothelial cells inducing pro-inflammatory genes. Previous studies have found that ROS can also affect the production of pro-inflammatory cytokines in endothelial cells, which can lead to endothelial dysfunction. The progression of atherosclerosis begins when an overabundance of ROS oxidizes LDL, and decreases the bioavailability of NO, leading to endothelial dysfunction [20].

Current Therapies for Atherosclerosis

Previous research suggests that pharmacotherapy may interfere with the progression of atherosclerosis in more than one mechanism. Statins are inhibitors of 3-hydroxy-3methylglutarylco-enzyme A (HMG-CoA) reductase. These drugs are suggested to lower the risk of developing CAD by lowering lipid levels, especially that of low-density lipoprotein (LDL). In Ortego et al. exposure of mononuclear cells and vascular smooth muscle cells with atorvastatin showed that atorvastatin reduced the activation of NF-κB, decreasing pro-inflammatory cytokines and chemokines that signal for endothelial inflammation [21, 22]. Although statins are effective in decreasing inflammation, they are also effective antioxidants that reduce ROS and atherosclerosis [21, 23-25]. However, they have also been linked to myalgia, diabetes, and neurological problems [26-30]. With atherosclerosis affecting over 90 million people in the U.S. alone, it is a major health concern. Although there are various therapeutic regimens, new treatments with minimal side effects are needed.

Carbon Nanoparticles

Pharmaceutical development has mainly been focused on drug delivery and drug efficacy. Appropriate drug delivery has limitations such as drug solubility, bio-distribution, biotransformation, toxicity and several side effects. Recently, the interdisciplinary research area of nanomedicine has gained attention. The nanotechnology and biomedical disciplines have set a focus in developing nanoparticles as a new drug delivery system to increase the bioavailability and efficacy of drugs by delivering them to targeted tissues [31]. Three types of carbon nanomaterial, graphene, nanotubes, and

fullerenes, have remained the main source of interest in research due to their size, semiconductor capacity, optical, and thermal properties. Carbon has multiple forms of allotropes such as diamond, graphite, and fullerene, which can all be used to produce carbon nanomaterial. This is known as the top-down synthesis. There are two main approaches in the synthesis for nanomaterial, bottom-up or top-down. Nanoparticle route synthesis can control the sample size distribution. The top-down is a harsh synthesis approach which breaks down the starting material into smaller particles, this however provides a wide size distribution. The bottom-up approach is using precursors to synthesize nanomaterial, this method provides a closer nanoparticle size distribution. An example of bottom-up synthesis is the synthesis of carbon nanotubes via graphene, a carbon allotrope which serves as the building block for fullerene and nanotube synthesis. A single layer of graphene, a layer of hexagonal lattice carbon atoms, can be manipulated to "wrap" and form fullerenes, and are "rolled" to produce carbon nanotubes [32]. Of the many classes of nanoparticles, carbon nanodots have become a novel area of interest due to their superior properties.

The discovery of quantum dots (QDs) was a major turning point in the synthesis of carbon nanodots. Quantum dots opened many potential bio-applications when they were discovered to have bright fluorescence, resistant to metabolic degradation, and were photo-stable. Quantum dots have been highly researched for their promising bioimaging properties. Negatively, their application is limited because of cellular toxicity, caused by heavy metals used in synthesis. They have also been documented to generate ROS, which activates the extrinsic and intrinsic apoptotic pathways [33, 34].

Carbon nanomaterial that contains carbon allotropes has been linked to DNA damage and cytotoxicity. Hizmann et al. analyzed cell toxicity and DNA damage when human glioblastoma U87 cells were exposed to different types of graphene. When cells were exposed to pristine graphene, and reduced graphene oxide, cell viability decreased, and DNA damage was observed [35]. With the discovery of carbon nanoparticles as promising therapeutic agents, biocompatibility and cytotoxicity need to be examined [36-38]. Diamond nanoparticles have also been promising bio-imaging agents, but studies had shown that when HeLa cells were exposed to diamond nanoparticles in serum-free media, high cytotoxicity was evident after 6 hours. Another study showed that diamond nanoparticles could damage the DNA of embryonic stem cells [39, 40]. While this may have some therapeutic effects for cancer treatment, it is necessary to reduce cytotoxic risk in healthy cells. The ideal carbon nanomaterial needs to have higher cell viability and retain QD properties for biomedical applications.

Carbon Nanodots (CNDs) Novel Nanoparticles

Carbon nanodots were accidentally discovered as fluorescent residue impurities after the synthesis of carbon nanotubes. They have a spherical or quasispherical structure, and their size is typically below 10nm. Carbon nanodots that are surface functional group rich have high solubility. Like QDs, they possess photoluminescence (PL) and rely on excitation, ranging from UV to visible light, and the emission produced may range from the UV to NIR light. Studies have linked CND photoluminescence to nanoparticle size and surface functional groups [41, 42]. By controlling the synthesis route used, different quantum yields (QY) may be acquired, resulting in different photoluminescence

properties. One method that has been adapted to the synthesis process is the use of molecules such as polyethylene glycol for surface passivation of CNDs to increase QY. Zhu et al. synthesized CNDs with citric acid and ethylenediamine as precursors, and the CNDs produced had a high QY of 80.6%, studies have also documented using precursors with amino groups to produce a high quantum yield [43-45] without the use of surface passivation. Unlike QDs, carbon nanodots use carbon precursors for synthesis (bottom-up synthesis), this is commonly referred to as green synthesis. Carbon nanodots have been documented to have low toxicity and high quantum yield which is relative to the emitted fluorescence.

This makes carbon nanodots candidates for biomedical applications such as therapeutic delivery and bio-imaging. With so many potential applications, the fine-tuning of carbon nanodot synthesis has been a major drive in all the research tangents regarding nanodots and medicine. For example, although advances in CND synthesis have been made, a major push is to develop carbon nanodots that can go into the nucleus. Previous studies have shown that most CNDs remain in the cytoplasm of cells after exposure [46, 47]. Nuclear targeting drug delivery would be optimal for cancer therapy, increasing the efficacy of drugs which have multiple side effects. However, it is known that positively charged CNDs are taken in by the cells, but only negatively charged CNDs could interact with the nucleus. This dilemma led to the fabrication of zwitterionic carbon nanodots that have functional groups with both charges to facilitate nuclear translocation.

Studies have also previously shown that carbon nanodots can track biological processes inside cells [48], deliver doxorubicin to cancer target cells [49, 50], and

scavenge radicals during oxidative stress [51, 52]. Das and colleagues synthesized CNDs from date molasses through microwave irradiation. After characterizing the nanomaterial, the biological application was tested on MG-63 human osteosarcoma cells. This synthesis not only showed high biocompatibility, but the carbon nanodots also showed high scavenging properties [53]. Zhang et al. used a single step microwave route to synthesize soluble carbon nanodots with citric acid and urea as precursors. Characterization of these carbon nanodots showed a spherical structure with an average size of 3nm with carboxylic and amino functional groups. Fluorescence emission spectrum was also analyzed in different wavelengths, and it was found that the highest emission peak was at an excitation peak of 360 nm with an emission peak of 454 nm. These same carbon nanodots were analyzed for antioxidant activity through the nitrogen-centered 2-2-diphenyl-1-picrylhydrazyl radical (DPPH•) assay which is a well-established assay used to measure antioxidant activity [54-56] by measuring the absorbance of DPPH•. The results showed that with increasing concentrations of CNDs, antioxidant activity increased, suggesting the potential bio-application of carbon nanodots in scavenging free radicals [57].

Atherosclerosis is an inflammatory disease that narrows the walls of the arteries via plaque buildup. Previous studies demonstrate that endothelial inflammation induced by TNFα plays a fundamental role in the initiation and progression of atherosclerosis. The transcriptional regulation of cytokines and vascular adhesion molecules are responsible for leukocyte adhesion to activated endothelial cells [58, 59]. Currently, there is not satisfactory anti-inflammatory drug therapy. With the incidence of cardiovascular

diseases expected to continue to increase, new treatments need to be developed. ROS are reactive free radicals containing oxygen and are known to play an important role in endothelial inflammation. Although previous studies have suggested the role of CNDs as free radical scavengers, the effect of carbon nanodots on the vascular system has not been reported, nor has its potential role in anti-inflammation against endothelial dysfunction.

The primary goal of this study was to investigate the role of CNDs in the modulation of TNFα-induced vascular inflammation both *in vitro* and *in vivo*. EA.hy926 was used as the *in vitro* cell model; this cell line is one of the best characterized vascular endothelial cell lines. These cells have been extensively used as a model for cardiovascular research to analyze expression of pro-inflammatory markers and leukocyte adhesion to activated cells. ApoE-/- mice have been used widely to study the pathophysiology of atherosclerosis. It is the most commonly used rodent model to examine events leading to plaque development and to test potential protective treatments for atherosclerosis [60-64]. I hypothesize that CNDs with antioxidant properties can protect against vascular inflammation. Accordingly, the study aims were designed to 1) examine *in vitro* carbon nanodot uptake and cytotoxicity in EA.hy926 endothelial cells; 2) investigate the role of CND in the modulation of TNFα-induced expression of pro-inflammatory genes and possible underlying mechanism(s); 3) examine the effects of carbon nanodots in Apo E-/- mice, a biological model of atherosclerosis. The possible impact of the role of carbon nanodots in vascular inflammation may provide new information on the potential application of carbon nanodots as an effective treatment for inflammatory disorders such as atherosclerosis.

CHAPTER II

MATERIALS AND METHODS

Materials

EA.hy926 endothelial cells from ATCC were purchased. For cell culturing Dulbecco's Modifies Eagles Medium (DMEM) were acquired from Gibco (12100-061), both the fetal bovine serum (FBS 26140-079) and penicillin streptomyosin (15140-122) were purchased from Gibco. For cell viability thiazolyl blue tetrazolium bromide was bought from Sigma (298-93-1), and Invitrogen molecular probe kit for flow cytometry was acquired (BMS306F1-300). PermaFluor Mountant for imaging came from ThermoFisher Scientific (TA-006-FM), and we used MitoTracker Red CMXRos manufactured by Life Technologies (M7512). For the purpose of gene expression the following reagents were purchased from Invitrogen; 10mM dNTP (18427-013), random primers (S8875), M-MLV reverse transcriptase (28025-013), 5X first strand buffer (Y02321). SYBR-Green was purchased from Applied Biosystems (4367659), and primer sequences (see sequences in qRT-PCR section) were sold by Eurofin. Apolipoprotein mice were obtained from Jackson Laboratory (002052).

Cell Culture

Human endothelial cells EA.hy926 were purchased from ATCC and grown in complete Dulbecco's Modifies Eagles Medium (DMEM) containing 10% fetal bovine serum and 1% penicillin-streptomycin. Cells were cultured in 72cm^2 Cellstar culture

flasks and kept in a humidified incubator at 37ºC and 5% CO_2. Cells were replenished with fresh media every two days; cells were passaged according to ATCC's sub-culturing procedure when cells were 90% confluent.

Carbon Nanodot (CND) Synthesis

Carbon-nanodots (CNDs) were synthesized by Wendy Zhang, a Ph.D. student in Dr. Jianjun Wei's lab at the Joint School of Nanoscience and Nanoengineering. The CNDs were synthesized by mixing 0.96g of citric acid (CA), 1 mL of Ethylenediamine (EDA) in 1 mL of deionized water. The solution was heated in a microwave synthesizer (CEM Corp 908005) at 300W for 10 minutes. To purify the CNDs, the solid was dissolved in DI water and dialyzed through a dialysis membrane with MWCO (molecular weight cut-out) of 1000Da for 24 hours.

Characterization of CND

Atomic force microscopy (AFM) was performed by JSNN to analyze morphology and size. To study the chemical content and the structure of the CNDs, Fourier transform infrared spectroscopy (FTIR) was done by JSNN. Using Cary fluorescence spectrophotometer, the fluorescence intensity peaks were measured to find the emission and excitation wavelengths for the carbon nanodots. The CND concentration in distilled water for analysis was 0.06 mg/mL.

CND Treatments

EA.hy296 cells were treated with CNDs with various concentrations for 24 hours in Hank's Balance Salt Solution (HBSS) media. Before treating cells with CNDs, cells

were rinsed with 7 mLs of 1X Phosphate Buffered Saline (PBS), the solution was decanted, and the treatment media was added.

CND Uptake Assay

Cells were treated at a time-dependent and dose-dependent manner. When treatment was over, treatment media was decanted, cells were rinsed twice with 7 mLs of 1X PBS. Cells were harvested using a cell scraper and centrifuged at 5000 rpm for 5 minutes at 4ºC. The supernatant was decanted, 900 µL of 1X PBS was used to suspend the cells. A black opaque 96 well plate was used to transfer 300 µL of suspended cells in technique triplicates. The plate was read using Synergy 2.0 well plate reader, fluorescence 360/460 top 400nm.

MTT Assay

EA.hy926 cells were cultured in a 48 well plate; cells were treated with 300 µL of various concentrations of carbon nanodots in HBSS media for 24 hours. After 24 hours, media was decanted, and cells were rinsed twice with 200 µL of 1X PBS. Low serum DMEM (0.5% FBS) was used to dilute 3-(4,5-dimethythiazol- 2-yl)-2,5-diphenyl tetrazolium bromide (MTT) to a concentration of 0.2 mg/mL. The treated cells were incubated with 300 µL of the diluted MTT; plates were kept in a humidified incubator at 37ºC and 5% CO_2 for 2 hours. After incubation, cells were rinsed with 1X PBS, and 300 µL of dimethyl sulfoxide (DSMO) was added. The plate was shaken at medium speed for 7 minutes before absorbance was measured using Synergy 2.0 plate reader at 570nm.

Flow Cytometry Assay

Cells were treated in HBSS media and various concentrations of carbon nanodots for 24 hours; treatment media was collected, cells were trypsinized, cold DMEM was used to neutralize trypsin and collected. Cells were centrifuged at 1000 rpm at 4ºC for 5 minutes. Cells were washed with PBS, counted, and centrifuged in Eppendorf centrifuge tubes at 5000 rpm at 4ºC for 5 minutes. The supernatant was decanted, the resulting pellet was re-suspended in the appropriate volume of 1X binding buffer to produce target cell concentration range of 1 x 10^5 and 1 x 10^6 cells per mL. In a flow cytometry tube, 100 µL of suspended cells were transferred, 5 µL of Annexin-V-FITC was added, followed by 1 µL of 7-AADD. Cells were kept in ice and incubated in the dark for 15 minutes. After incubation 400 µL of the 1X binding buffer was added to the cells and samples were analyzed using Guava® easyCyte Flow Cytometer.

Quantitative Real Time Polymerase Chain Reaction

EA.hy926 cells were treated with CNDs only and 0.5ng TNFα co-treatments. Cells were rinsed after treatment, and 1 mL of RNA isolation reagent was added to the treatment plate. Cells and solution were then transferred to a microcentrifuge tube and incubated for 5 minutes at room temperature (RT). After incubation, 200 µL of chloroform was added, followed by a 3 min RT incubation. The RNA extraction supernatant was then spun at 12000 rcf for 15 min at 4ºC. The aqueous phase was transferred to another tube, and 500 µL of isopropanol was added and incubated for 10mins RT. The supernatant was centrifuged at 12000 rcf for 10 min at 4ºC. The supernatant was decanted, and RNA pellet was washed twice with 1 mL 75% ethanol,

spun at 7400 rcf for 5 min at 4ºC. On the last wash, the supernatant was decanted, and the tube was inverted to air dry for 10 mins. The RNA pellet was eluted in 15 µL of DEPC water and incubated for 20 mins RT. RNA concentration was quantified, and cDNA was made after RNA was diluted to 500 ng/µL. Gene primer master mix was made, cDNA was diluted to a 1:9 ratio with DEPC water, 19 µL of the gene master mix was used per well, and 1µL of cDNA was used to plate.

Table 1. Sequences of Primers Used For qRT-PCR.

Primers and Sequences		
Target Gene	**Forward (5'-3')**	**Reverse (3'-5')**
GAPDH	CGACCACTTTGTCAAGCTCA	AGGGGTCTACATGGCAACTG
CCL2	CCCCAGTCACCTGCTGTTAT	TGGAATCCTGAACCCACTTC
ICAM	GGCTGGAGCTGTTTGAGAAC	ACTGTGGGGTTCAACCTCTG
IL-8	TAGCAAAATTGAGGCCAAGG	AAACCAAGGCACAGTGGAAC

Cell Fixation of CND Treatments

Cells were grown on cover slips and treated for 24 hours with various CND concentrations in HBSS media. Cover slips were washed three times in 1X PBS twice and incubated in 3.7% PFA for 7 minutes. Cover slips were rinsed twice with 1X PBS following PFA fixation. To mount cover slips to slides, 15µl of PermaFluor Mountant media was used. Slides were left over night to set. Imaging was done using the Keyence BZ-X710 fluorescence microscope.

Cell Fixation of MitoTracker Red and CNDs

Cells on coverslips were treated with CNDs for 24 hr in HBSS media. Cells were stained with MitoTracker Red and incubated with the stain 30 minutes prior to the end of the 24 hr CND treatment. Cells were washed three times with 1X PBS, incubated in 3.7% PFA for 7 minutes, cover slips were rinsed twice with 1X PBS. Cover slips were mounted onto slides using 15 µl of PermaFluor Mountant media. Slides were left over night in the dark to set; imaging was done with Keyence BZ-X710 fluorescence microscope.

Antioxidant Sample Preparation

Treated EA.hy926 endothelial cells were harvested by decanting the media, rinsing twice with sterile 1X PBS. Cells were then trypsinized using 1.5 mL of trypsin and incubated for 3-5 mins. Trypsin was canceled by adding 7 mLs of complete DMEM containing 10% fetal bovine serum; the collected cells were then centrifuged at 1000 rpm for 7 minutes at 4ºC. The pellet was suspended in 1 mL of PBS, transferred to a microcentrifuge tube and spun at 5000 rpm for 5 minutes at 4ºC. PBS was decanted and the pellet was suspended in 250 µL of tissue buffer (60Mm K_2HPO_4/KH_2PO_4 + 1mM EDTA pH 7.4 + 0.1% Triton-100). Cells were sonicated three times for 15 seconds with a 5 second resting period in between. The sonicated cells were spun at 13000 rpm for 10 minutes at 4ºC. The antioxidant supernatant was transferred to a sterile microcentrifuge tube and stored at -80ºC.

Total Protein Assay

Pierce Coomassie (Bradford) Protein Dye was used for this assay, 800 µL of the dye was added to a test tube followed by 6 µL of antioxidant sample. For the standard, 10 µL of BSA 1.48mg/mL was used the final volume in each test tube was 800 µL. Absorbance was read at 595nm.

Total NADPH Quinone Oxidoreductase-1 (NQO1) Assay

Antioxidant sample lysate was used for the assay. Light sensitive NQO1 reaction mixture was made using 12 mLs NQO1 Buffer (50mM Tris-HCL, 0.08% TritonX-100 pH 7.5); 48 µL of 20 mM dichlorophenolindophenol (DCPIP) and 36 µL of 50mM nicotinamide adenine dinucleotide phosphate (NADPH). In a cuvette, 698 µL of the NQO1 reaction mixture and 2 uL of antioxidant lysate sample was added, inverted and immediately measured. Total NQO1 was obtained by reading the absorbance (600nm every 15 seconds for 3 minutes) using DU800 spectrophotometer.

Glutathione Reductase (GR) Assay

Antioxidant lysate samples were used for this assay. In a cuvette, 465 µL of GR buffer (50mM K_2HPO_4/KH_2PO_4 1mM EDTA pH 7.0), 60 µL of 20mM GSSG, and 15 µL of the antioxidant sample (tissue buffer for blank) were added. The assay mixture was incubated for 3 minutes at 37 ºC in the DU800 spectrophotometer. After incubation, 60 µL of 1.5Mm NADPH was added, cuvettes were inverted with parafilm and read at 37 ºC, 340nm, 30-second intervals for 5 minutes.

Glutathione S-Transferase (GST) Assay

Light sensitive GST reaction mixture was made with 10 mL GST buffer (0.1M K_2HPO_4/KH_2PO_4 pH 6.5), 30mg of bovine serum albumin (BSA), 200 µL of 50mM 1-chloro-2,4-dinitrobenzene (CDNB) in ethanol, and 100 µL of 100mM GSH. DU800 spectrophotometer was blanked with a cuvette containing 585 µL of the reaction mixture and 15 µL of tissue buffer. Antioxidant lysate samples were used for this assay. Each cuvette for each sample contained 585 µL of the reaction mixture and 15 µL of the sample. The cuvette was inverted to mix the sample and read at 340nm every 30 seconds for 5 minutes at 25ºC.

Animal Dosing

Thirty-six 5-week-old male ApoE-/- mice were purchased from the Jackson Laboratory. Mice were randomly placed in cages (3 animals per cage), and held in isolation for one week. The animals were fed an atherogenic diet (15% fat by weight; 0.25% cholesterol, Harlan Teklad) one week prior to animal dosing. Cages were picked at random for dosing, CNDs were diluted to the desired concentrations with sterile saline. All mice were dosed daily via intraperitoneal injection for eight weeks. All experimental mice were dosed in the same manner given different concentrations of carbon nanodots in saline (0.1 mg/kg BW, 0.1 mg/kg BW, 0.5 mg/kg BW, 2.5 mg/kg BW). Mice were fed atherogenic diet for the duration of this study. After the 8-week dosing period was over, animals were humanely euthanized with isoflurane, and the cardiac puncture was performed afterward, along with cervical dislocation. Tissue samples were collected

including aorta, kidneys, brain, heart, spleen, etc. Selected samples were placed in 10% buffered formaldehyde for histopathological examination.

Histology Assessment of Kidney, Liver and Aorta

Three samples per experimental group were collected for the liver, kidney, and aorta histology. Hematoxylin and eosin tissue slides were prepared by AML Laboratories. Imaging of the samples was done using Keyence BZ-X710. Images were sent to collaborators at Michigan State Medical School and analyzed by our collaborator Robert Sigler DVM, Ph.D., ACVP, Clinical Professor and Director, In-Vivo Animal Core.

CHAPTER III

RESULTS

Characterization of CNDs

Carbon nanoparticle synthesis provides unique features [40-42] to nanomaterial. The nanoparticles used in this study possess their own fluorescence. Prior to conducting experiments, we verified the photoluminescence characterization of carbon nanodots through ultraviolet-visible spectrophotometry (Fig 1A). The excitation and emission of CNDs at a concentration of 0.06 mg/mL was measured to be 350 nm and 461 nm respectively. The fluorescence of nanomaterial can be excitation-independent or excitation-dependent. To further verify the photoluminescence properties, we measured the emission of 0.06 mg/mL CNDs for the following wavelengths; 320 nm, 340 nm, 360 nm, 380 nm, 400 nm, and 420 nm. Figure 2A shows that the emission peaks for different excitations are found at about 460 nm, verifying that the synthesized carbon nanodots are excitation independent.

CND Uptake in EA.hy926 Endothelial Cells

Photoluminescent characterization was important for our experiments to study CND uptake using fluorescence microscopy. Using the excitation and emission spectra of carbon nanodots, fluorescence imaging was done after a 24 hr exposure of 0.6 mg/mL CNDs in EA.hy926 endothelial cells. The DAPI channel was used to observe

fluorescence in EA.hy926 cells after CND exposure. Figure 2A shows that as expected, the control group does not have fluorescence under the DAPI channel. The cells treated with 0.6 mg/mL CND for 24 hr show fluorescence, indicating that the nanomaterial goes into the cells. To further verify if there was a change in fluorescence with increasing concentration exposure of CNDs EA.hy926 cells were exposed to 0 mg/mL, 0.3 mg/mL, 0.6 mg/mL, and 1.2 mg/mL of CNDs (Fig. 2B). Panel B shows a visible increase in fluorescence that is dose-dependent. Prior to quantifying the amount of carbon nanodots that enter the cells, a carbon nanodot standard was created by measuring the fluorescence of known concentrations (Fig. 3C). A line of regression was created and used to calculate CND uptake. As shown in figure 4A, EA.hy926 cells were treated with various concentrations of CNDs for 24 hr and uptake was quantified. CND uptake with the tested concentrations was found to be dose-dependent. CND uptake analysis shows that nanomaterial uptake is also time-dependent (Fig. 3B).

Cell Viability Determined by MTT Assay

Any substance has the potential to be toxic when the chemical reaches a sufficient concentration. The effect of carbon nanodots on cell viability was measured through MTT assay, which measures a cell's metabolic activity {Riss, 2004 #106}. The CND concentrations used to analyze cell viability through MTT were 0 mg/mL, 0.0003 mg/mL, 0.003 mg/mL, 0.03 mg/mL, 0.3 mg/mL, 0.6 mg/mL, and 1.2 mg/mL. Hydrogen peroxide, known to affect metabolic activity was used as the positive control {Cossu, 2012 #126}. Cell viability was analyzed in a time-dependent manner. Figure 4A shows that after a 3 hr incubation when compared to the control, cell viability does not change.

After 6 hr CND exposure (Fig 4B), the highest concentration shows cytotoxicity. As shown in Fig 4C, EA.hy926 endothelial cells treated with 0.6 mg/mL and 1.2 mg/mL CND show a decrease of 9.8% and 14.5% in cell viability after 12 hr incubation. Following a 24 hr exposure to CNDs, 0.6 mg/mL and 1.2 mg/mL showed significant cytotoxicity compared to the control (Fig 4D).

Cell Viability Determined by Flow Cytometry

To further confirm the effect of carbon nanodots on cell viability, the Annexin-FITC flow cytometry assay was used to analyze cells undergoing apoptosis and necrosis. Cells undergoing apoptosis are identified through the binding of the Annexin V-FITC conjugate to phosphatidylserine, a phospholipid cell membrane component normally located in the inner leaflet of the membrane that translocates to the outer surface during apoptosis. The conditions used for flow cytometry are the same used to analyze cell viability through MTT assay. Figure 5A shows EA.hy926 cell viability after a 12 hr CND exposure; there is no cell viability difference between the control and the CND treatments. Flow cytometry plots are read in the following manner; the viable cells are plotted in the bottom left quadrant, the cells undergoing early apoptosis are in the bottom left quadrant. The top left quadrant is where necrotic cells are a plot, and the top right quadrant is where late apoptotic cells are plotted. As depicted in figure 5B, after a 24 hr incubation period with varying CND concentrations, there is a significant cell viability decrease of 20% in the highest CND concentration used when compared to the control.

Fluorescence Imaging of Mitochondria and CNDs

Cells were treated with 0 mg/mL, 0.3 mg/mL, 0.6 mg/mL, AND 1.2 mg/mL of CNDs for 24 hr, mitochondria were stained with MitoTracker Red for 30 min. Fluorescence imaging was done as seen in figure 6. Imaging was done for both the mitochondria and the CNDs with the use of different channels in the fluorescence microscope, followed by the overlay imaging.

Effects of CNDs on TNF-α-Induced Expression of Pro-Inflammatory Genes

Atherosclerosis is an inflammatory disease mediated by pro-inflammatory markers. Therefore we used qRT-PCR to measure the effects that CNDs have on TNF-α-induced mRNA levels of several pro-inflammatory genes. EA.hy926 cells were co-treated with 0.5 ng TNF-α and increasing concentrations of CNDs for 24 hr. Figure 7A shows an increase in the relative gene expression of CCL2 induced by co-treatment. Compared to TNF-α, 0.003 mg/mL and increasing concentrations of CND co-treatments show a significant increase in gene expression. ICAM gene expression (Fig 7B) shows a statistically significant decrease in all co-treatments when compared to TNF-α-induced expression of ICAM. As shown in figure 6C, there is a significant decrease in mRNA levels of IL-8 in the higher concentration of CND co-treatments when compared to TNF-α only.

Effects of CNDs Alone on Expression of Pro-Inflammatory Genes

After analyzing mRNA levels of co-treatment with TNF-α, it was crucial to analyze the effect of CNDs alone on pro-inflammatory markers of atherosclerosis. We

studied the effect of gene expression with increasing concentrations of carbon nanodots in EA.hy926 cells for 24 hr. Figure 8A shows that there are CND dosages that decrease the levels of CCL2 mRNA. The gene expression for ICAM (Fig 8B) shows that 0.03 mg/mL significantly reduces the expression of ICAM after 24 hr. Interleukin-8 mRNA levels are affected after 24 hr by CNDs concentrations of 0.0003 mg/mL, and 0.03 mg/mL (Fig 8C).

Increase in NOQ1 Activity by Carbon Nanodots After 24 hr

To further examine intracellular effects of CNDs we measured the activity of phase II detoxifying enzymes that are important to xenobiotic biotransformation and excretion. Cells were treated for 24 hr with 0 mg/mL, 0 mg/mL, 0.0003 mg/mL, 0.003 mg/mL, 0.03 mg/mL, 0.3 mg/mL of CNDs and samples were prepared to measure the activity of phase II detoxifying enzymes through enzyme kinetic assays. NQO1 activity was significantly increased in 0.0003 mg/mL, 0.003 mg/mL, and 0.03 mg/mL of CND treatments, as seen in figure 9A. The activity of glutathione s-transferase (Fig 9B), and glutathione reductase (9C) did not differ from the control.

Carbon Nanodots Have No Effect in Apo E -/- Mice Body Weight (BW)

Apo E -/- mice are a biological model for atherosclerosis pathophysiology. Mice were dosed daily with CNDs for 8 weeks via intraperitoneal dosing (0 mg/mL BW, 0.1 mg/mL BW, 0.5 mg/mL BW, 2.5 mg/mL BW). Body weight of every group was recorded. The values shown are the body weight at the end of the week. Week (-1) shows the weight of the animals before they were fed the atherogenic diet, week zero showed

the body weight of the groups when dosing started. When compared to the control group for the week, carbon nanodots do not affect body weight as shown in figure 10.

Histology Assessment of the Aorta, Kidney, and Liver

Samples were sent to AML Laboratories for processing and hematoxylin and eosin staining. Figure 11 shows that the aorta of wild-type mice (C57BL/6 mice) appear to have normal aorta. Apo E -/- show a structural irregularity of the aorta, and accumulation of fibrous tissue. Whereas the aorta of CND dosed mice may show a decrease in aortic plaque formation. Histological samples of the liver show swollen hepatocytes and lipid accumulation. Samples from mice dosed with CNDs have a visible decrease in hepatic lipidosis (Fig 12). Imaging for kidney histology across all experimental groups seems to be unchanged compared to the wild-type mice (Fig 13).

CHAPTER IV

DISCUSSION

The leading cause of death worldwide is cardiovascular disease. The silent progression of plaque formation on blood vessels, or atherosclerosis, causes ischemia leading to more pathological cardiovascular diseases such as coronary artery disease (CAD), myocardial infarction (MI), transient ischemic attack (TIA), and acute coronary syndrome (ACS). The epidemiology of the cardiovascular disease is a universal health concern driving research for novel treatment options. Nanomedicine is the application of nanoparticles, the material below 100 nm in size, for medical purposes. This interdisciplinary field has been a growing in the last decade, increasing the classes of nanoparticles synthesized, as well as improving the synthesis technique [36, 65-67]. Carbon nanodots are a new class of nanoparticles that are prospective candidates for medical applications.

In this study, we have demonstrated that the emission peaks of citric acid-ethylenediamine (CA-EDA) synthesized carbon nanodots under different excitations are at about 460 nm, suggesting that the photoluminescence properties of this nanoparticle are excitation independent. Our results are consistent with previous reports that carbon nanodots can be excitation independent according to the synthesis method [36, 43, 65, 66]. This excitation independent photoluminescence property (Fig 1A, 1B), allows for the

analysis of carbon nanodot uptake in EA.hy926 endothelial cells. Using spectrofluorometric measurement, our study demonstrated that nanodot uptake is both time and concentration dependent in endothelial cells (Fig. 3A, 3B). Carbon nanodot uptake by endothelial cells was further verified through fluorescence microscopy. Currently, there is limited literature in evaluating cellular uptake of carbon nanodot into living cells. In this context, our results present for the first-time, direct evidence that carbon nanodot can enter the cell at a concentration as low as 0.03 ng/mL. The question that remains unanswered is how carbon nanodots enter endothelial cells. Quantum dots have been documented to enter HeLa cancer cells through macropinocytosis and cell receptor-mediated endocytosis [68, 69]. Due to shared characteristics, it remains under investigation whether the entry mechanism of carbon nanodots in the endothelial cells is like that of quantum dots in HeLa cancer cells.

The cell membrane protects intracellular components against the surrounding environment. When xenobiotics enter cells, they may cause toxic or adverse effect if the levels reach high concentrations. Although previous studies have documented cytotoxicity of CNDs in different cell lines, cytotoxicity has not been analyzed in endothelial cells. Thus, it is important to determine not only potential toxic concentrations, but also the mechanism of toxicity of CNDs to endothelial cells. The first assay used to analyze cell viability was the MTT assay, which measures cell viability through metabolic activity. Our MTT results showed that carbon nanodot concentrations of up to 0.3 mg/mL do not affect cell viability for up to 24 hr (Fig 4D). It was observed that highest concentration of carbon nanodots used (1.2 mg/mL) caused a decrease in cell

viability after 6hr (Fig. 4B), and 0.6 mg/mL of CNDs shows cytotoxicity as early as 12 hr after exposure (Fig. 4C). To further confirm the effects of CNDs on endothelial cell viability, the Annexin V-FITC with 7-AAD flow cytometry assay was further used. Cell viability through flow cytometry revealed that after 24 hr, only 1.2 mg/mL of CND decreases cell viability through apoptosis (Fig. 5A). Thus, these results do not parallel our results from the MTT assay. While 0.6 mg/mL of CND was not shown to affect cell viability via the flow cytometry assay, the same concentration showed a decrease in metabolic activity after 12 hr using MTT assay. The highest concentration of carbon nanodots tested showed a decrease in cell viability via flow cytometry after 24 hr exposure (Fig. 5B), whereas with the MTT assay detected a significant decrease in cell viability after 6 hr.

These inconsistent results are mainly due to different viability assays. Through the Annexin V conjugate assay, cells undergoing apoptosis are identified through the binding of the Annexin V-FITC conjugate to phosphatidylserine, which translocates from the inner leaflet of the membrane to the outer surface during apoptosis. In contrast, the MTT assay is dependent on the ability of a healthy cell to undergo mitochondrial reductase to convert MTT to formazan crystals, which can be visualized as purple crystals inside the cell. Therefore, this assay reflects metabolic cellular activity or mitochondrial function, rather than direct cell viability. In this context, our data shows that higher concentrations of CNDs may directly target on the mitochondria, disrupting cellular metabolic activity. Indeed, previous studies report that mitochondrion are reported to be one of the first sites to be affected by many xenobiotics [70, 71].

To further investigate the above phenomenon, the EA.hy926 endothelial cells were labeled with MitoTracker Red, which labels metabolically active mitochondria following treatment with various concentrations of CNDs. Fluorescence microscopy images were then taken of CND, and of the labeled mitochondria followed by overlay images of the CND and mitochondria fluorescence (Fig. 6). Our results demonstrated that it is likely that the location of CNDs and the mitochondria overlap, however, due to limitations of fluorescence microscopy, further analysis should be done through confocal microscopy to assess if CNDs and mitochondria co-localize, affecting cell viability. With confocal microscopy, the sample can be sectioned, decreasing off-focus imaging, and overlap with different channels can verify co-localization [72].

Since Inflammation-induced mononuclear cell adhesion to activated endothelium lining is crucial for atherosclerosis, this study further analyzed the effect of CNDs on TNFα-induced endothelial inflammation. Previous studies demonstrate that TNFα-induced endothelial inflammation plays a fundamental role in the initiation and progression of atherosclerosis. TNFα is a homotrimer cell signaling protein, or cytokine, which is known to activate the endothelium, creating an inflammatory response. Pro-inflammatory mediators that play a crucial role in the progression of atherosclerosis are cytokines and surface adhesion molecules such as interleukin 8 (IL-8), intracellular adhesion molecule 1 (ICAM-1) and monocyte chemoattractant protein-1 (MPC-1/CCL2) [7-10]. Previous studies show that the gene expression decrease in IL-8 can reduce the progression of atherosclerosis [73-75]. The expression of ICAM-1 and other vascular adhesion molecules on the surface of endothelial cells is crucial to the progression of

plaque development because of their roles in firm monocyte adhesion to the damaged endothelium. ICAM-1 can bind to the function-associated antigen (LFA-1) on activated leukocytes; this process helps leukocytes migrate to the tunica intima [76]. Thus, these molecules have been widely accepted as excellent biomarkers of vascular dysfunction [77-80].

Concurrent to previous studies [81, 82], our studies showed that exposure of EA.hy926 endothelial cells to TNF-α significantly induced the expression of IL-8, ICAM-1, and MPC-1/CCL2 indicating the critical role of these chemokines/adhesion molecules in TNF-α-induced vascular inflammation. TNF-α-induced IL-8 expression is decreased significantly with increasing CND exposure suggesting the decrease in IL-8 to activate and recruit leukocytes to the site of inflammation. Likewise, CND concentrations as low as 0.3 ng/mL also inhibited TNF-α -induced ICAM-1 expression. These results demonstrated the anti-inflammatory effect of CNDs in a dose-dependent manner. However, it remains to be investigated why the expression of MPC-1/CCL2 was increased with CND exposure. Also, our data showed that carbon nanodots alone could decrease basal levels of the target genes studied, suggesting that CNDs can decrease the basal inflammatory response.

Studies have shown that NF-κB, a transcription factor, is crucial in regulating the expression of endothelial adhesion molecules and pro-inflammatory mediators which increase leukocyte adhesion and migration to the site of the dysfunctional endothelium [11, 12]. The inactive form of NF-κB is associated with the cytoplasmic inhibitory protein Ik-B in the inactive form. Xenobiotic stimulation can result in the degradation of

Ik-B, translocating the p50/65 heterodimer to the nucleus, and upregulating transcription of pro-inflammatory genes [83, 84]. In the development of atherosclerosis, TNFα induces the activation of NF-κB increasing the expression of pro-inflammatory genes which modulate leukocyte adhesion to damaged endothelium. However, it remains unknown if CNDs can protect vasculature against inflammation induced by TNF-α, via the NF-κB pathway.

Aside from the nuclear translocation of NF-κB, endothelial dysfunction can be elicited by reactive oxygen species (ROS) such as superoxide, hydrogen peroxide, hydroxyl radical, and peroxynitrite [85-87]. These reactive oxygen species have been shown to regulate NF-κB activation through TNF-α and other pro-inflammatory cytokines [88]. Interestingly, TNF-α-induced vascular inflammation releases of both superoxide and hydrogen peroxide [89]. A main target of ROS is the oxidation of LDL. The oxidation of LDL is an important event in the accumulation of plaque because it is ingested by macrophages to form a prominent characteristic of plaque, the formation of foam cells [85-87]. Important antioxidants in vasculature that protect against oxidative stress by quenching ROS include glutathione (GSH), NQO1, GST and GR [90]. NQO1 is a cytoprotective enzyme, one of its many known functions include the 2 electron reduction of quinines, along with decreasing the radical formation of semiquinones and the resulting ROS [91]. An additional function is to sustain the levels of important antioxidants like ubiquinone and vitamin E by reducing their derivatives to antioxidants [92, 93]. It has also been established that NQO1 scavenges superoxide anion radicals, protecting vasculature from oxidative stress [91, 94]. Interestingly, studies have shown

that in cardiovascular tissue, NQO1 is expressed much higher levels than in other tissue types [95] . This project was also the first to study the effects of CNDs on antioxidant enzymatic activity in EA.hy926 endothelial cells. Interestingly, our results show that only the activity of NQO1 increased (Fig. 9A). In agreement with previous studies outlining the significant role of NQO1 in the maintenance of vascular homeostasis [96], our data suggests that NQO1 may be a cytoprotective mechanism of carbon nanodots to protect against TNFα-induced endothelial inflammation. However, it is unclear how CNDs increases cellular NQO1 activity in endothelial cells. Activation of nuclear factor erythroid 2–related factor 2 (Nrf2)/Keap-1/ARE signaling has been proposed in concurrent studies, to play an important role in in expression of intracellular NQO-1 [97]. Further investigation is required to examine the nuclear translocation of Nrf2 to understand the effect of carbon nanodots on NQO1 enzyme activity. Understanding the mechanism of action by which carbon nanodots activate NOQ1 is important due to the important role of NOQ1 in regulating healthy vascular homeostasis.

This project was also the first to study the effects of CNDs in atherosclerosis *in vivo.* Apolipoprotein E deficient (Apo E -/-) mice are the animal model most widely used for atherosclerosis. Apolipoprotein E is a protein that is synthesized in the liver, the most important role of this protein is to transport cholesterol and lipids to different tissues. The deficiency of apolipoprotein E increases cholesterol levels in the bloodstream as it impairs the clearance of cholesterol by the liver [98]. To study the effects of CNDs in atherosclerosis Apo E -/- mice, different carbon nanodot dosages were given daily via intraperitoneal dosing for 8 weeks. The body weight was monitored weekly, and after 8

weeks of dosing, the mice were euthanized, and hematoxylin and eosin samples of the aorta, kidney, and liver were prepared and examined. The chronic inflammatory response to the damaged endothelial lining of vessels can cause the progressive accumulation of plaque in vessels which can be observed in the Apo E -/- mice aorta. Our results show that there may be a decrease in plaque formation in the aorta of Apo E -/- mice dosed with CNDs as compared to the Apo E deficient mice, suggesting that CNDs can ameliorate vascular function in atherosclerosis. Apolipoprotein E deficiency has been linked to an increase in oxidative stress [99, 100], which can lead to the oxidation of macromolecules, and the damage to vascular endothelial damage. In this context, the CND protective effect could be partially due to the scavenging properties of the carbon nanodots[24, 25, 79], which can protect the endothelium. The liver is important for cholesterol homeostasis, but it is also an important organ that metabolizes a major quantity of xenobiotics or drugs via the first pass effect before it reaches the bloodstream [101]. Our histology imaging shows lipid accumulation in Apo E knockout mice, which could be due to the inability to excrete cholesterol into bile. *Consistent* to our findings for the aorta, CND treatment appears to reduce hepatic lipid accumulation compared to the Apo E knockout mice. However, CND treatment did not affect on in kidney. In addition to our findings, the CND treatment did not affect the body weight of the Apo E -/- mice, which is consistent with previous animal studies that reported no significant body weight change or toxic effect on BALB/c mice dosed with 2.5 mg/mL of CNDs [102, 103] suggesting the safety of carbon nanodots.

In summary, our study provided a biological characterization of citric acid, and EDA synthesized nanodots *in vitro* and *in vivo* via EA.hy926 endothelial cells and Apo E knockout mice. Utilizing the intrinsic fluorescence of CND, it was found that incubation of EA.hy926 cells with CND resulted in a dose and time-dependent intracellular uptake of this nanoparticle. Higher concentrations of carbon nanodots seem to affect cellular viability through targeting mitochondria metabolic activity. However future studies should be designed to analyze the relationship between mitochondria and carbon nanodots. CND significantly inhibited TNF-α-mediated expression of IL-8 and adhesion molecule ICAM-1, two key molecules that are responsible for the activation and the firm adhesion of monocytes to activated endothelial cells for the initiation of atherosclerosis. CND treatment also increased the activity of NQO1 in EA.hy926 endothelial cells. In the animal study, it is suggested that the plaque formation in the aorta and hepatic lipid accumulation in the Apo E knockout mice are reduced with CND dosing. Our studies suggest that the anti-inflammatory effect of CND was likely due to the scavenging properties of CNDs and the upregulation of NQO1 activity (Fig. 14). However, the exact molecular mechanisms involved are largely unknown and remain to be investigated. To further understand the effect of carbon nanodots beyond that of atherosclerosis, the pharmacodynamics and pharmacokinetics need to be explored. The possible impact of carbon nanodots on vascular inflammation may provide new information on the future application of carbon nanodots as an effective treatment for inflammatory disorders such as atherosclerosis.

REFERENCES

1. Go, A.S., et al., *Heart disease and stroke statistics--2014 update: a report from the American Heart Association.* Circulation, 2014. **129**(3): p. e28-e292.

2. Benjamin, E.J., et al., *Heart Disease and Stroke Statistics-2017 Update: A Report From the American Heart Association.* Circulation, 2017. **135**(10): p. e146-e603.

3. International, R., *Cardiovascular disease: A costly burden for America projections through 2035* 2017, American Heart Association: American Heart Association. p. 16.

4. Gaziano, T.A., *Reducing the growing burden of cardiovascular disease in the developing world.* Health Aff (Millwood), 2007. **26**(1): p. 13-24.

5. WHO. *Cardiovascular Disease*. 2017 2017; Available from: http://www.who.int/cardiovascular_diseases.

6. Zalba, G., et al., *Vascular oxidant stress: molecular mechanisms and pathophysiological implications.* J Physiol Biochem, 2000. **56**(1): p. 57-64.

7. Pearson, T.A., et al., *Markers of inflammation and cardiovascular disease: application to clinical and public health practice: A statement for healthcare professionals from the Centers for Disease Control and Prevention and the American Heart Association.* Circulation, 2003. **107**(3): p. 499-511.

8. Thompson, S.G., et al., *Hemostatic factors and the risk of myocardial infarction or sudden death in patients with angina pectoris. European Concerted Action on Thrombosis and Disabilities Angina Pectoris Study Group.* N Engl J Med, 1995. **332**(10): p. 635-41.

9. Danesh, J., et al., *C-reactive protein and other circulating markers of inflammation in the prediction of coronary heart disease.* N Engl J Med, 2004. **350**(14): p. 1387-97.

10. Ridker, P.M., et al., *C-reactive protein and other markers of inflammation in the prediction of cardiovascular disease in women.* N Engl J Med, 2000. **342**(12): p. 836-43.

11. Sun, Y. and L.W. Oberley, *Redox regulation of transcriptional activators.* Free Radic Biol Med, 1996. **21**(3): p. 335-48.

12. Brand, K., et al., *Activated transcription factor nuclear factor-kappa B is present in the atherosclerotic lesion.* J Clin Invest, 1996. **97**(7): p. 1715-22.

13. Kunsch, C. and R.M. Medford, *Oxidative stress as a regulator of gene expression in the vasculature.* Circ Res, 1999. **85**(8): p. 753-66.

14. Williams, K.J. and I. Tabas, *The response-to-retention hypothesis of early atherogenesis.* Arterioscler Thromb Vasc Biol, 1995. **15**(5): p. 551-61.

15. Gimbrone, M.A., Jr., T. Nagel, and J.N. Topper, *Biomechanical activation: an emerging paradigm in endothelial adhesion biology.* J Clin Invest, 1997. **99**(8): p. 1809-13.

16. Topper, J.N., et al., *Identification of vascular endothelial genes differentially responsive to fluid mechanical stimuli: cyclooxygenase-2, manganese superoxide dismutase, and endothelial cell nitric oxide synthase are selectively up-regulated by steady laminar shear stress.* Proc Natl Acad Sci U S A, 1996. **93**(19): p. 10417-22.

17. Griendling, K.K., D. Sorescu, and M. Ushio-Fukai, *NAD(P)H oxidase: role in cardiovascular biology and disease.* Circ Res, 2000. **86**(5): p. 494-501.

18. Laursen, J.B., et al., *Endothelial regulation of vasomotion in apoE-deficient mice: implications for interactions between peroxynitrite and tetrahydrobiopterin.* Circulation, 2001. **103**(9): p. 1282-8.

19. Negre-Salvayre, A., et al., *Advanced lipid peroxidation end products in oxidative damage to proteins. Potential role in diseases and therapeutic prospects for the inhibitors.* Br J Pharmacol, 2008. **153**(1): p. 6-20.

20. Incalza, M.A., et al., *Oxidative stress and reactive oxygen species in endothelial dysfunction associated with cardiovascular and metabolic diseases.* Vascul Pharmacol, 2018. **100**: p. 1-19.

21. Lin, R., et al., *Lovastatin reduces nuclear factor kappaB activation induced by C-reactive protein in human vascular endothelial cells.* Biol Pharm Bull, 2005. **28**(9): p. 1630-4.

22. Ortego, M., et al., *Atorvastatin reduces NF-kappaB activation and chemokine expression in vascular smooth muscle cells and mononuclear cells.* Atherosclerosis, 1999. **147**(2): p. 253-61.

23. Beltowski, J., *Statins and modulation of oxidative stress.* Toxicol Mech Methods, 2005. **15**(2): p. 61-92.

24. Stoll, L.L., et al., *Antioxidant effects of statins.* Timely Top Med Cardiovasc Dis, 2005. **9**: p. E1.

25. Pratico, D., *Antioxidants and endothelium protection.* Atherosclerosis, 2005. **181**(2): p. 215-24.

26. Brosteaux, C., et al., *[Statins and muscular side-effects].* Rev Med Suisse, 2010. **6**(239): p. 510, 512-4, 516-7.

27. Carter, A.A., et al., *Risk of incident diabetes among patients treated with statins: population based study.* BMJ, 2013. **346**: p. f2610.

28. Preiss, D., et al., *Risk of incident diabetes with intensive-dose compared with moderate-dose statin therapy: a meta-analysis.* JAMA, 2011. **305**(24): p. 2556-64.

29. Rajpathak, S.N., et al., *Statin therapy and risk of developing type 2 diabetes: a meta-analysis.* Diabetes Care, 2009. **32**(10): p. 1924-9.

30. Sinzinger, H., R. Wolfram, and B.A. Peskar, *Muscular side effects of statins.* J Cardiovasc Pharmacol, 2002. **40**(2): p. 163-71.

31. Perry, J.L., C.R. Martin, and J.D. Stewart, *Drug-delivery strategies by using template-synthesized nanotubes.* Chemistry, 2011. **17**(23): p. 6296-302.

32. Geim, A.K. and K.S. Novoselov, *The rise of graphene.* Nat Mater, 2007. **6**(3): p. 183-91.

33. Chen, N., et al., *The cytotoxicity of cadmium-based quantum dots.* Biomaterials, 2012. **33**(5): p. 1238-44.

34. Nguyen, K.C., et al., *Mitochondrial Toxicity of Cadmium Telluride Quantum Dot Nanoparticles in Mammalian Hepatocytes.* Toxicol Sci, 2015. **146**(1): p. 31-42.

35. Hinzmann, M., et al., *Nanoparticles containing allotropes of carbon have genotoxic effects on glioblastoma multiforme cells.* Int J Nanomedicine, 2014. **9**: p. 2409-17.

36. Liu, H., et al., *Microwave-assisted synthesis of wavelength-tunable photoluminescent carbon nanodots and their potential applications.* ACS Appl Mater Interfaces, 2015. **7**(8): p. 4913-20.

37. Park, S.Y., et al., *Advanced carbon dots via plasma-induced surface functionalization for fluorescent and bio-medical applications.* Nanoscale, 2017. **9**(26): p. 9210-9217.

38. Zhang, X., et al., *A cytotoxicity study of fluorescent carbon nanodots using human bronchial epithelial cells.* J Nanosci Nanotechnol, 2013. **13**(8): p. 5254-9.

39. Li, J., et al., *Nanodiamonds as intracellular transporters of chemotherapeutic drug.* Biomaterials, 2010. **31**(32): p. 8410-8.

40. Xing, Y., et al., *DNA damage in embryonic stem cells caused by nanodiamonds.* ACS Nano, 2011. **5**(3): p. 2376-84.

41. Kong, B., et al., *Carbon dot-based inorganic-organic nanosystem for two-photon imaging and biosensing of pH variation in living cells and tissues.* Adv Mater, 2012. **24**(43): p. 5844-8.

42. Sharma, A., et al., *Origin of Excitation Dependent Fluorescence in Carbon Nanodots.* J Phys Chem Lett, 2016. **7**(18): p. 3695-702.

43. Zhu, S., et al., *Highly photoluminescent carbon dots for multicolor patterning, sensors, and bioimaging.* Angew Chem Int Ed Engl, 2013. **52**(14): p. 3953-7.

44. Chen, P.C., et al., *Photoluminescent organosilane-functionalized carbon dots as temperature probes.* Chem Commun (Camb), 2013. **49**(16): p. 1639-41.

45. Yang, Y., et al., *One-step synthesis of amino-functionalized fluorescent carbon nanoparticles by hydrothermal carbonization of chitosan.* Chem Commun (Camb), 2012. **48**(3): p. 380-2.

46. Arvizo, R.R., et al., *Effect of nanoparticle surface charge at the plasma membrane and beyond.* Nano Lett, 2010. **10**(7): p. 2543-8.

47. Mehiri, M., et al., *Cellular entry and nuclear targeting by a highly anionic molecular umbrella.* Bioconjug Chem, 2008. **19**(8): p. 1510-3.

48. Depeng Kong, F.Y., Yunmei Luo, Yinyin Wang, Li Chen and Fenghai Cui, *Carbon nanodots prepared for cellular imaging and turn-on detection of glutathione.* Analytical Methods, 2016. **8**(23): p. 4736-4743.

49. Tang, J., et al., *Carbon nanodots featuring efficient FRET for real-time monitoring of drug delivery and two-photon imaging.* Adv Mater, 2013. **25**(45): p. 6569-74.

50. Wang, S., et al., *Augmented glioma-targeted theranostics using multifunctional polymer-coated carbon nanodots.* Biomaterials, 2017. **141**: p. 29-39.

51. Xu, Z.Q., et al., *Highly Photoluminescent Nitrogen-Doped Carbon Nanodots and Their Protective Effects against Oxidative Stress on Cells.* ACS Appl Mater Interfaces, 2015. **7**(51): p. 28346-52.

52. Kamakshi Bankoti, A.P.R., Sayanti Datta, Bodhisatwa Das, Analava Mitra and Santanu Dhara, *Onion derived carbon nanodots for live cell imaging and accelerated skin wound healing.* 2017. **5**(32): p. 6579-6592.

53. Das, B., et al., *Carbon Nanodots from Date Molasses: New Nanolight to Scavenge Reactive Oxygen Species In Vitro*. Vol. 2. 2014.

54. Kato, K., et al., *Studies on scavengers of active oxygen species. 1. Synthesis and biological activity of 2-O-alkylascorbic acids.* J Med Chem, 1988. **31**(4): p. 793-8.

55. Mehtab Parveen, F.A., Ali Mohammed Malla, Shaista Azaz, *Microwave-assisted green synthesis of silver nanoparticles from Fraxinus excelsior leaf extract and its antioxidant assay.* Applied Nanoscience, 2016. **6**(2): p. 267–276.

56. Blois, M.S., *Antioxidant Determinations by the Use of a Stable Free Radical.* Nature, 1958. **181**: p. 1199-1200.

57. Zhang, W., Z. Zeng, and J. Wei, *Electrochemical Study of DPPH Radical Scavenging for Evaluating the Antioxidant Capacity of Carbon Nanodots.* The Journal of Physical Chemistry C, 2017. **121**(34): p. 18635-18642.

58. Levine, B., et al., *Elevated circulating levels of tumor necrosis factor in severe chronic heart failure.* N Engl J Med, 1990. **323**(4): p. 236-41.

59. Hallenbeck, J.M., *The many faces of tumor necrosis factor in stroke.* Nat Med, 2002. **8**(12): p. 1363-8.

60. Plump, A.S., et al., *Severe hypercholesterolemia and atherosclerosis in apolipoprotein E-deficient mice created by homologous recombination in ES cells.* Cell, 1992. **71**(2): p. 343-53.

61. Piedrahita, J.A., et al., *Generation of mice carrying a mutant apolipoprotein E gene inactivated by gene targeting in embryonic stem cells.* Proc Natl Acad Sci U S A, 1992. **89**(10): p. 4471-5.

62. Meir, K.S. and E. Leitersdorf, *Atherosclerosis in the apolipoprotein-E-deficient mouse: a decade of progress.* Arterioscler Thromb Vasc Biol, 2004. **24**(6): p. 1006-14.

63. Coleman, R., et al., *A mouse model for human atherosclerosis: long-term histopathological study of lesion development in the aortic arch of apolipoprotein E-deficient (E0) mice.* Acta Histochem, 2006. **108**(6): p. 415-24.

64. Whitman, S.C., *A practical approach to using mice in atherosclerosis research.* Clin Biochem Rev, 2004. **25**(1): p. 81-93.

65. Liu, J., et al., *One-step hydrothermal synthesis of photoluminescent carbon nanodots with selective antibacterial activity against Porphyromonas gingivalis.* Nanoscale, 2017. **9**(21): p. 7135-7142.

66. Park, S.Y., et al., *Photoluminescent green carbon nanodots from food-waste-derived sources: large-scale synthesis, properties, and biomedical applications.* ACS Appl Mater Interfaces, 2014. **6**(5): p. 3365-70.

67. Chen, B., et al., *Large scale synthesis of photoluminescent carbon nanodots and their application for bioimaging.* Nanoscale, 2013. **5**(5): p. 1967-71.

68. Ruan, G., et al., *Imaging and tracking of tat peptide-conjugated quantum dots in living cells: new insights into nanoparticle uptake, intracellular transport, and vesicle shedding.* J Am Chem Soc, 2007. **129**(47): p. 14759-66.

69. Osaki, F., et al., *A quantum dot conjugated sugar ball and its cellular uptake. On the size effects of endocytosis in the subviral region.* J Am Chem Soc, 2004. **126**(21): p. 6520-1.

70. Kumar, P., A. Nagarajan, and P.D. Uchil, *Analysis of Cell Viability by the MTT Assay.* Cold Spring Harb Protoc, 2018. **2018**(6): p. pdb prot095505.

71. Marks, D.C., et al., *The MTT cell viability assay for cytotoxicity testing in multidrug-resistant human leukemic cells.* Leuk Res, 1992. **16**(12): p. 1165-73.

72. Dunn, K.W., M.M. Kamocka, and J.H. McDonald, *A practical guide to evaluating colocalization in biological microscopy.* Am J Physiol Cell Physiol, 2011. **300**(4): p. C723-42.

73. Apostolakis, S., et al., *Interleukin 8 and cardiovascular disease.* Cardiovasc Res, 2009. **84**(3): p. 353-60.

74. Latruffe, N., et al., *Exploring new ways of regulation by resveratrol involving miRNAs, with emphasis on inflammation.* Ann N Y Acad Sci, 2015. **1348**(1): p. 97-106.

75. Rezaie-Majd, A., et al., *Simvastatin reduces expression of cytokines interleukin-6, interleukin-8, and monocyte chemoattractant protein-1 in circulating monocytes from hypercholesterolemic patients.* Arterioscler Thromb Vasc Biol, 2002. **22**(7): p. 1194-9.

76. Kurokouchi, K., et al., *TNF-alpha increases expression of IL-6 and ICAM-1 genes through activation of NF-kappaB in osteoblast-like ROS17/2.8 cells.* J Bone Miner Res, 1998. **13**(8): p. 1290-9.

77. Hansson, G.K., *Immune and inflammatory mechanisms in the pathogenesis of atherosclerosis.* J Atheroscler Thromb, 1994. **1 Suppl 1**: p. S6-9.

78. Libby, P., P.M. Ridker, and A. Maseri, *Inflammation and atherosclerosis.* Circulation, 2002. **105**(9): p. 1135-43.

79. Mangge, H., et al., *Antioxidants, inflammation and cardiovascular disease.* World J Cardiol, 2014. **6**(6): p. 462-77.

80. Collins, T., *Endothelial nuclear factor-kappa B and the initiation of the atherosclerotic lesion.* Lab Invest, 1993. **68**(5): p. 499-508.

81. Tak, P.P. and G.S. Firestein, *NF-kappaB: a key role in inflammatory diseases.* J Clin Invest, 2001. **107**(1): p. 7-11.

82. Pamukcu, B., et al., *The role of monocytes in atherosclerotic coronary artery disease.* Ann Med, 2010. **42**(6): p. 394-403.

83. Xie, W. and Y. Tian, *Xenobiotic receptor meets NF-kappaB, a collision in the small bowel.* Cell Metab, 2006. **4**(3): p. 177-8.

84. Zhou, C., et al., *Mutual repression between steroid and xenobiotic receptor and NF-kappaB signaling pathways links xenobiotic metabolism and inflammation.* J Clin Invest, 2006. **116**(8): p. 2280-2289.

85. Hansson, G.K., *Inflammation, atherosclerosis, and coronary artery disease.* N Engl J Med, 2005. **352**(16): p. 1685-95.

86. Ross, R., *Atherosclerosis--an inflammatory disease.* N Engl J Med, 1999. **340**(2): p. 115-26.

87. Steinberg, D., *Atherogenesis in perspective: hypercholesterolemia and inflammation as partners in crime.* Nat Med, 2002. **8**(11): p. 1211-7.

88. Gloire, G., S. Legrand-Poels, and J. Piette, *NF-kappaB activation by reactive oxygen species: fifteen years later.* Biochem Pharmacol, 2006. **72**(11): p. 1493-505.

89. Radeke, H.H., et al., *Interleukin 1-alpha and tumor necrosis factor-alpha induce oxygen radical production in mesangial cells.* Kidney Int, 1990. **37**(2): p. 767-75.

90. Stocker, R. and J.F. Keaney, Jr., *Role of oxidative modifications in atherosclerosis.* Physiol Rev, 2004. **84**(4): p. 1381-478.

91. Ross, D., et al., *NAD(P)H:quinone oxidoreductase 1 (NQO1): chemoprotection, bioactivation, gene regulation and genetic polymorphisms.* Chem Biol Interact, 2000. **129**(1-2): p. 77-97.

92. Ross, D., *Quinone reductases multitasking in the metabolic world.* Drug Metab Rev, 2004. **36**(3-4): p. 639-54.

93. Siegel, D., et al., *The reduction of alpha-tocopherolquinone by human NAD(P)H: quinone oxidoreductase: the role of alpha-tocopherolhydroquinone as a cellular antioxidant.* Mol Pharmacol, 1997. **52**(2): p. 300-5.

94. Zhao, Q., et al., *Unexpected genetic and structural relationships of a long-forgotten flavoenzyme to NAD(P)H:quinone reductase (DT-diaphorase).* Proc Natl Acad Sci U S A, 1997. **94**(5): p. 1669-74.

95. Zhu, H., et al., *The highly expressed and inducible endogenous NAD(P)H:quinone oxidoreductase 1 in cardiovascular cells acts as a potential superoxide scavenger.* Cardiovasc Toxicol, 2007. **7**(3): p. 202-11.

96. Isbir, C.S., et al., *The effect of NQO1 polymorphism on the inflammatory response in cardiopulmonary bypass.* Cell Biochem Funct, 2008. **26**(4): p. 534-8.

97. Itoh, K., et al., *Keap1 regulates both cytoplasmic-nuclear shuttling and degradation of Nrf2 in response to electrophiles.* Genes Cells, 2003. **8**(4): p. 379-91.

98. Greenow, K., N.J. Pearce, and D.P. Ramji, *The key role of apolipoprotein E in atherosclerosis.* J Mol Med (Berl), 2005. **83**(5): p. 329-42.

99. Shea, T.B., et al., *Apolipoprotein E deficiency promotes increased oxidative stress and compensatory increases in antioxidants in brain tissue.* Free Radic Biol Med, 2002. **33**(8): p. 1115-20.

100. Ramassamy, C., et al., *Impact of apoE deficiency on oxidative insults and antioxidant levels in the brain.* Brain Res Mol Brain Res, 2001. **86**(1-2): p. 76-83.

101. Urso, R., P. Blardi, and G. Giorgi, *A short introduction to pharmacokinetics.* Eur Rev Med Pharmacol Sci, 2002. **6**(2-3): p. 33-44.

102. Wang, K., et al., *Systematic safety evaluation on photoluminescent carbon dots.* Nanoscale Res Lett, 2013. **8**(1): p. 122.

103. Gao, Z., et al., *Carbon dots: a safe nanoscale substance for the immunologic system of mice.* Nanoscale Res Lett, 2013. **8**(1): p. 276.

APPENDIX A

FIGURES

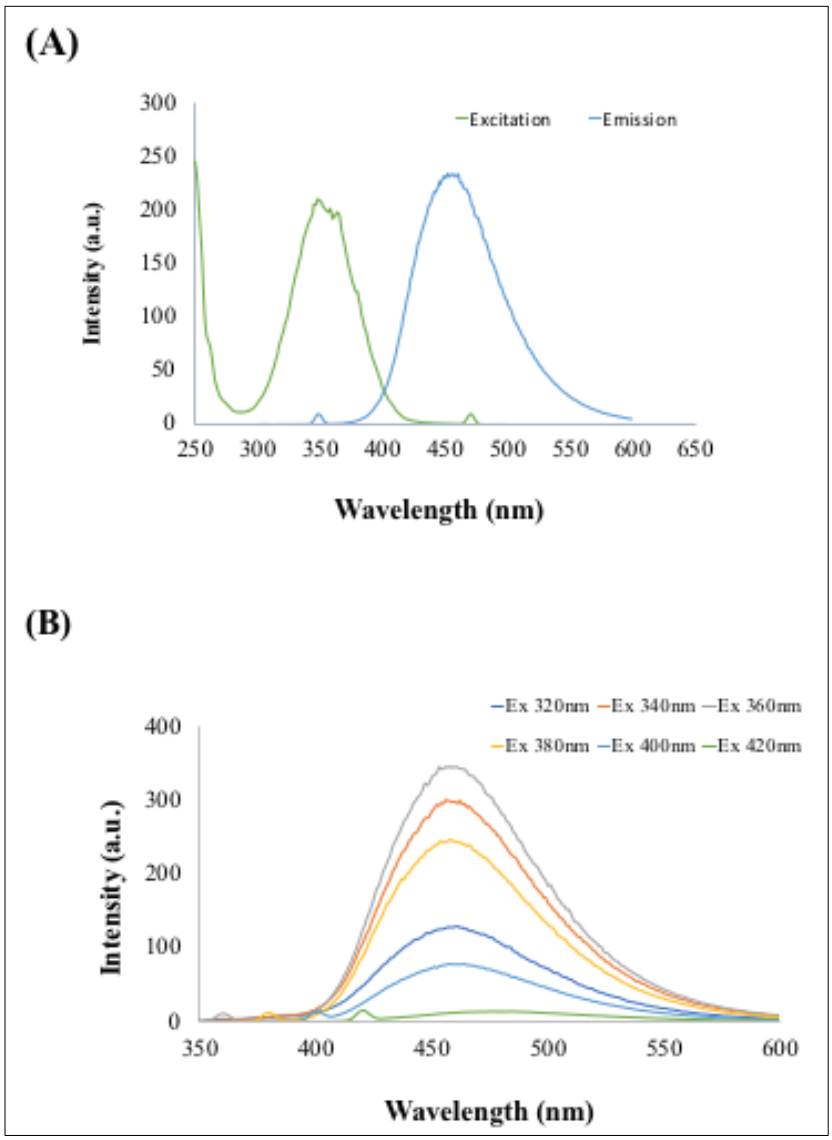

***Figure 1*. Characterization of CNDs.** *(A) Excitation and emission of carbon nanodots were characterized using Cary fluorescence spectrophotometer. Excitation intensity peak is at 350nm, and emission intensity peak is at 461nm. (B) CNDs are excitation independent; the emission was analyzed after CNDs were tested at several excitation wavelengths. The highest emission is reached at 360nm.*

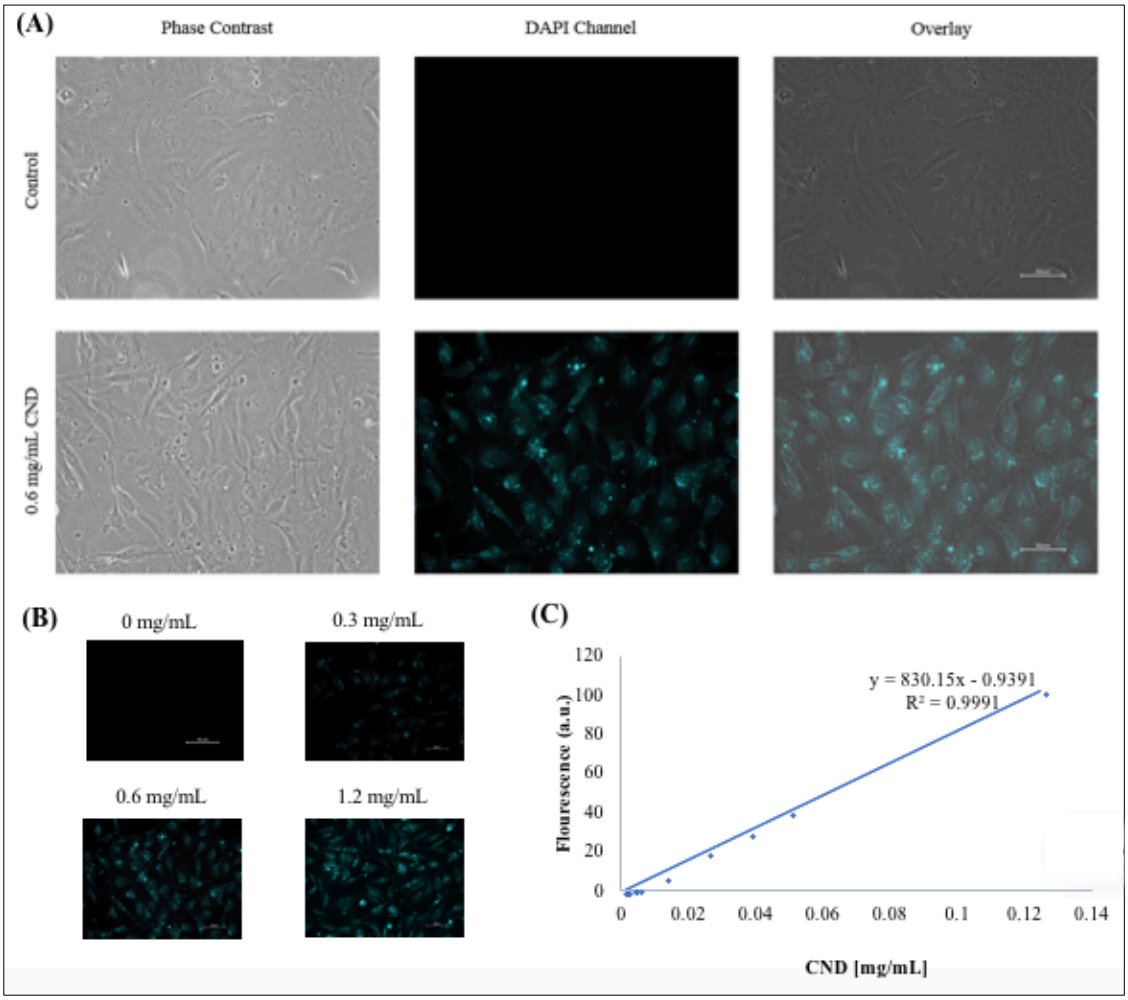

Figure 2. Fluorescence Microscopy of CND Treated Endothelial Cells. ***(A) Fluorescence microscopy images of EA.hy926 human endothelial cells treated 0.6mg/mL CNDs for 24 hr.*** *Carbon nanodot excitation and emission are similar to those used for the DAPI channel. Overlay image for the control shows no fluorescence; the CND treated cells shows fluorescence after 24 hr. Cells were imaged using Keyence microscope.* ***(B) Fluorescence in EA.hy926 human endothelial cells treated with increasing concentrations of CNDs after 24 hr exposure.*** *Panel A shows an increase in fluorescence with increasing concentrations, top left: control; top right: 0.3 mg/mL; bottom left: 0.6 mg/mL; bottom right: 1.2 mg/mL. Cells were imaged using Keyence microscope.* ***(C) CND standard curve used to quantify CND uptake****. The fluorescence of known concentrations of CNDs was measured in a microplate reader, a line of regression was created to calculate nanomaterial uptake in cells.*

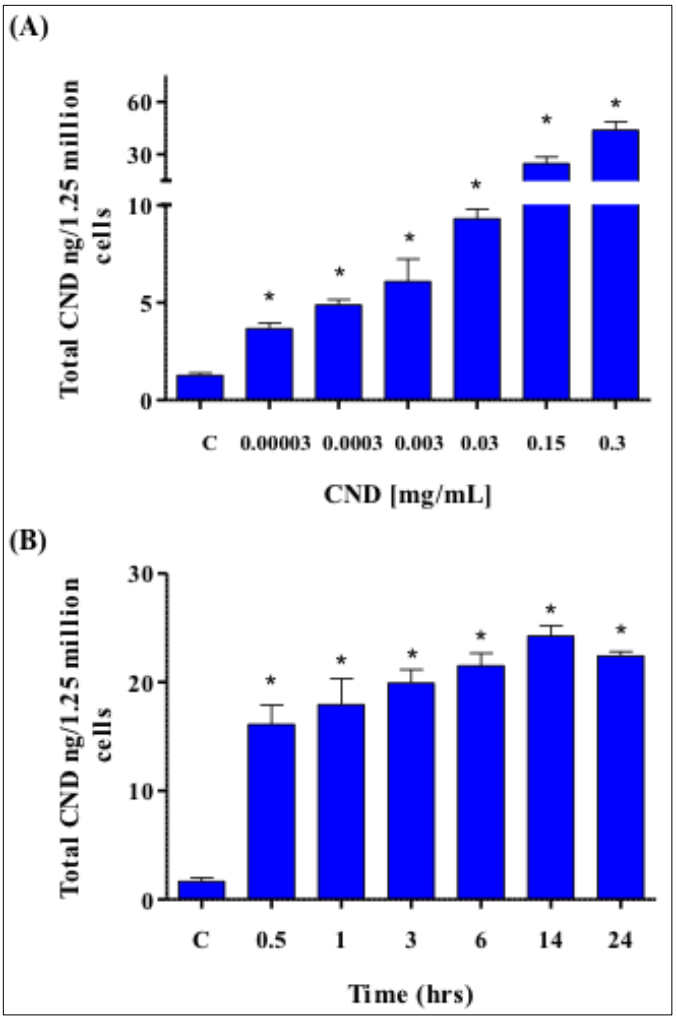

Figure 3. EA.hy926 Endothelial Cellular Uptake of CNDs. *(A) Concentration-dependent exposure of CNDs in endothelial cells. EA.hy926 endothelial cells were treated with CNDs in HBSS media in a concentration-dependent manner for 24 hrs. (B) Time-dependent analysis of CND uptake of endothelial cells exposed to 0.15 mg/mL. Fluorescence was quantified via Bio-Tek Synergy 2.0 microplate reader. Nanodot uptake was calculated through the use of a standard curve. All data represent mean ± SEM (n=3), T-test data analysis *p<0.05 vs. control.*

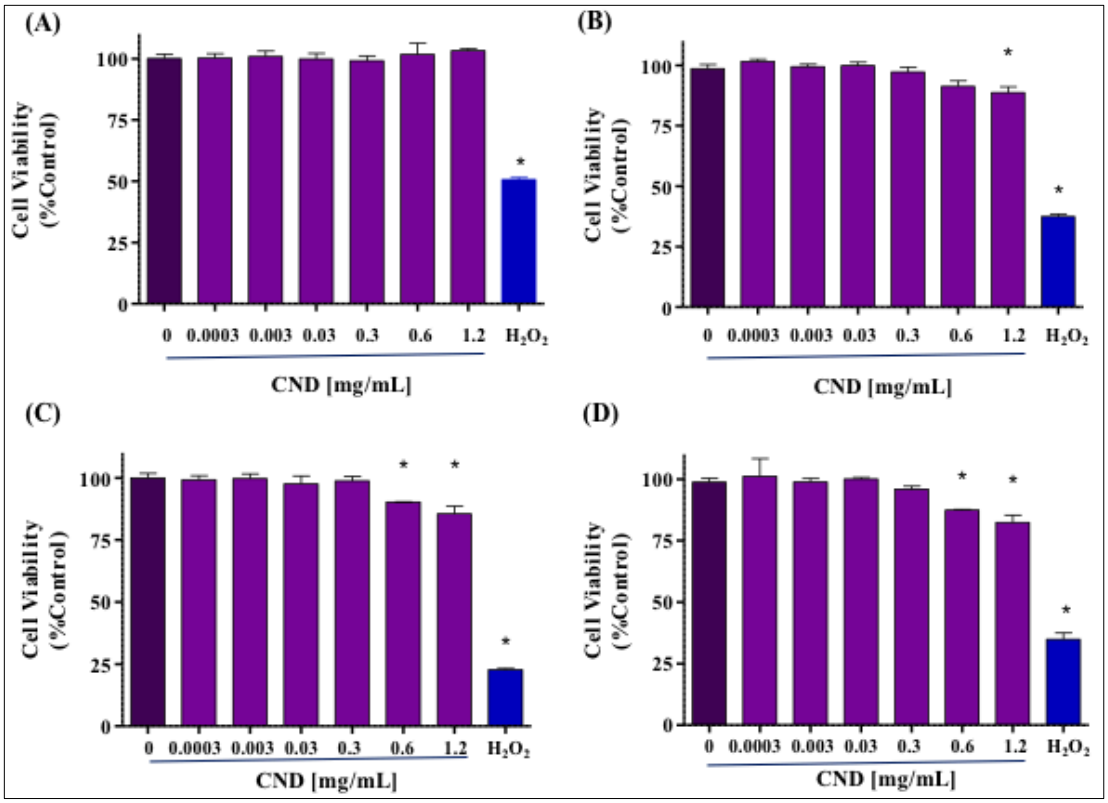

Figure 4. Cell Viability Determined by Colorimetric MTT Assay*. EA.hy926 cells were treated with various concentrations of CNDs in HBSS media. H_2O_2 was used as a positive control. (A) Low and high concentrations of CNDs were used to treat endothelial cells for 3 hrs. (B) 6 hr carbon nanodot treatment on endothelial cells shows that the at 1.2 mg/mL cell viability decreases. (C) Endothelial cells were treated with CNDs for 12 hr, compared to the control, only the cell viability for highest concentration is statistically significant. (D) After 24 hr exposure to CNDs 0.6 mg/mL 1.2 mg/mL are cytotoxic to endothelial cells. Data shown are mean ± SEM (n=3), 1- Way ANOVA, *p<0.05 vs. control.*

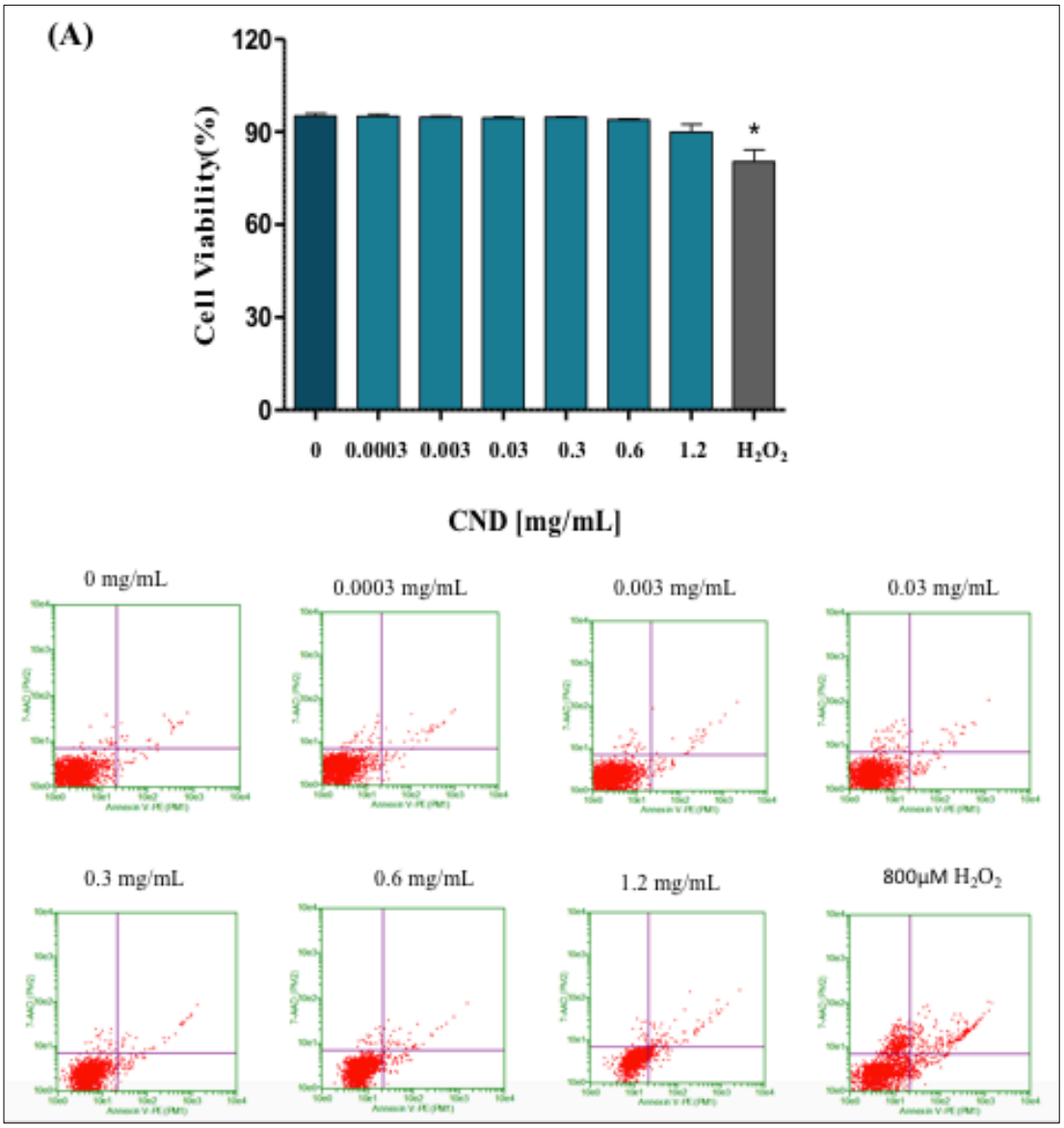

Figure 5A. Cell Viability Analyzed Through the Annexin-FITC Flow Cytometry Assay After 12 hr Exposure. *(A) EA.hy926 endothelial cells were exposed for 12 hr with various carbon nanodot concentrations; cell viability was quantified through the Nexin flow cytometry assay. Top row from left to right) control, 0.0003mg/mL CND, 0.003mg/mL CND, 0.03mg/mL, (bottom row from left to right) 0.3mg/mL, 0.6mg/mL, 1.2 mg/mL CND, 800μM H_2O_2 0 as the positive control treatments. When compared to the control, no condition was statistically significant. Data shown are mean ± SEM (n=3), 1-Way ANOVA, *p<0.05 vs. control.*

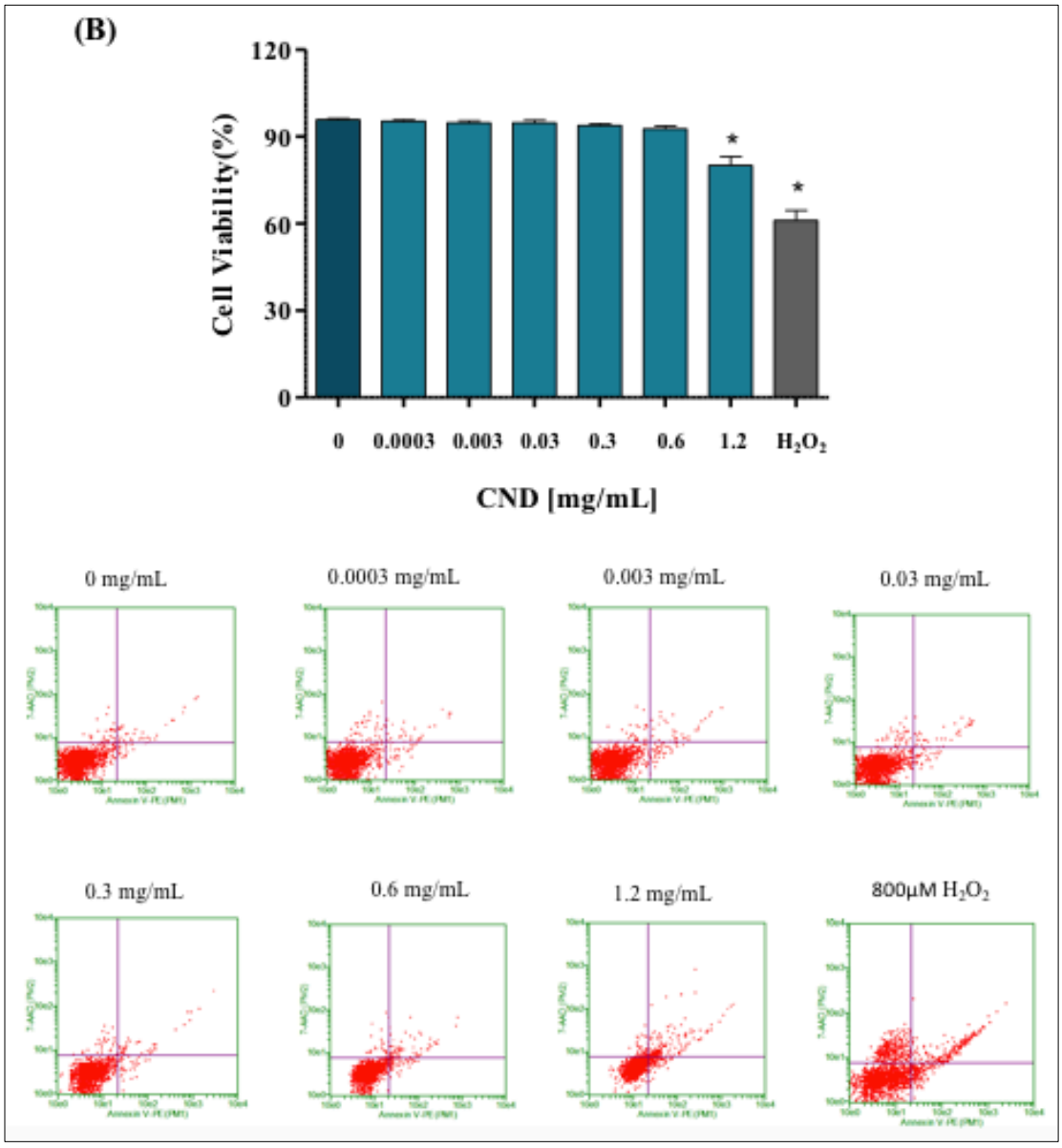

Figure 5B. Cell Viability Analyzed Through the Annexin-FITC Flow Cytometry Assay After 24 hr Exposure. *EA.hy926 cells were treated with HBSS media for 24 hours for the (top row from left to right) control, 0.0003mg/mL CND, 0.003mg/mL CND, 0.03mg/mL, (bottom row from left to right) 0.3mg/mL, 0.6mg/mL, 1.2 mg/mL CND, 800µM H_2O_2 0 as the positive control treatments. Cell viability for 1.2 mg/mL CND was the only condition that was statistically significant when compared to the control. Flow cytometry plots are shown to the right; quantified cell viability graph is on the left. Data shown are mean ± SEM (n=3), 1- Way ANOVA, *p<0.05 vs. control.*

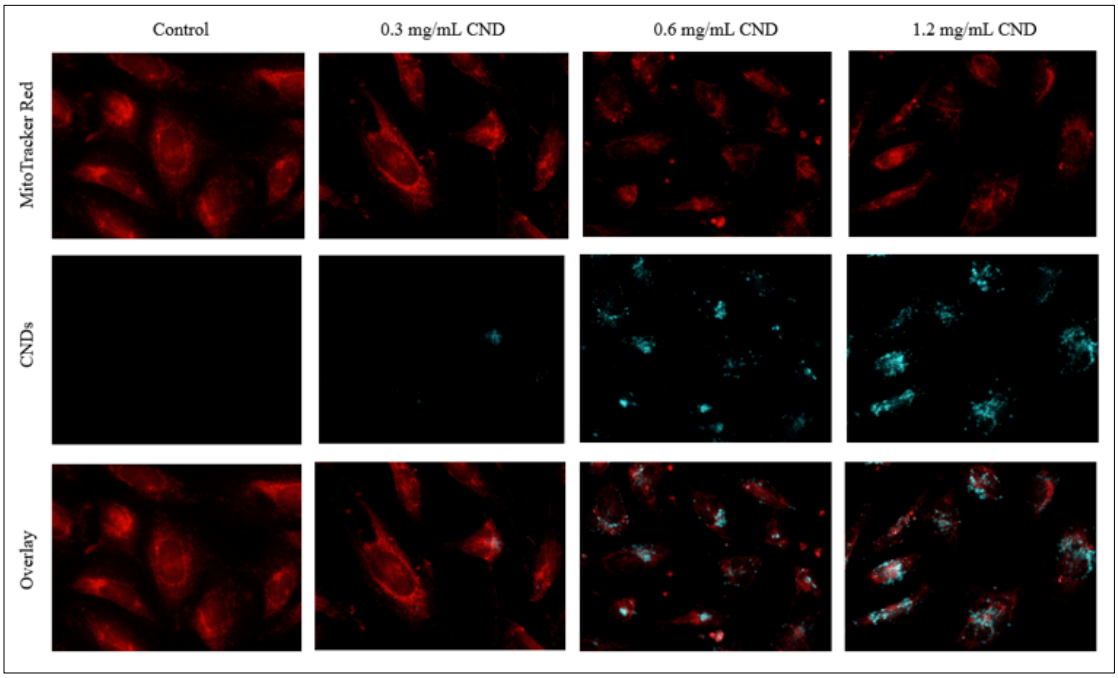

Figure 6. Fluorescence Imaging of CNDs and Mitochondria in EA.hy926 Endothelial Cells. *Cells were exposed to 0.3 mg/mL, 0.6 mg/mL, and 1.2 mg/mL carbon nanodots for 24 hr in HBSS media. MitoTracker Red was used to label active mitochondria. Keyence BZ-710 fluorescence microscope was used for imaging.*

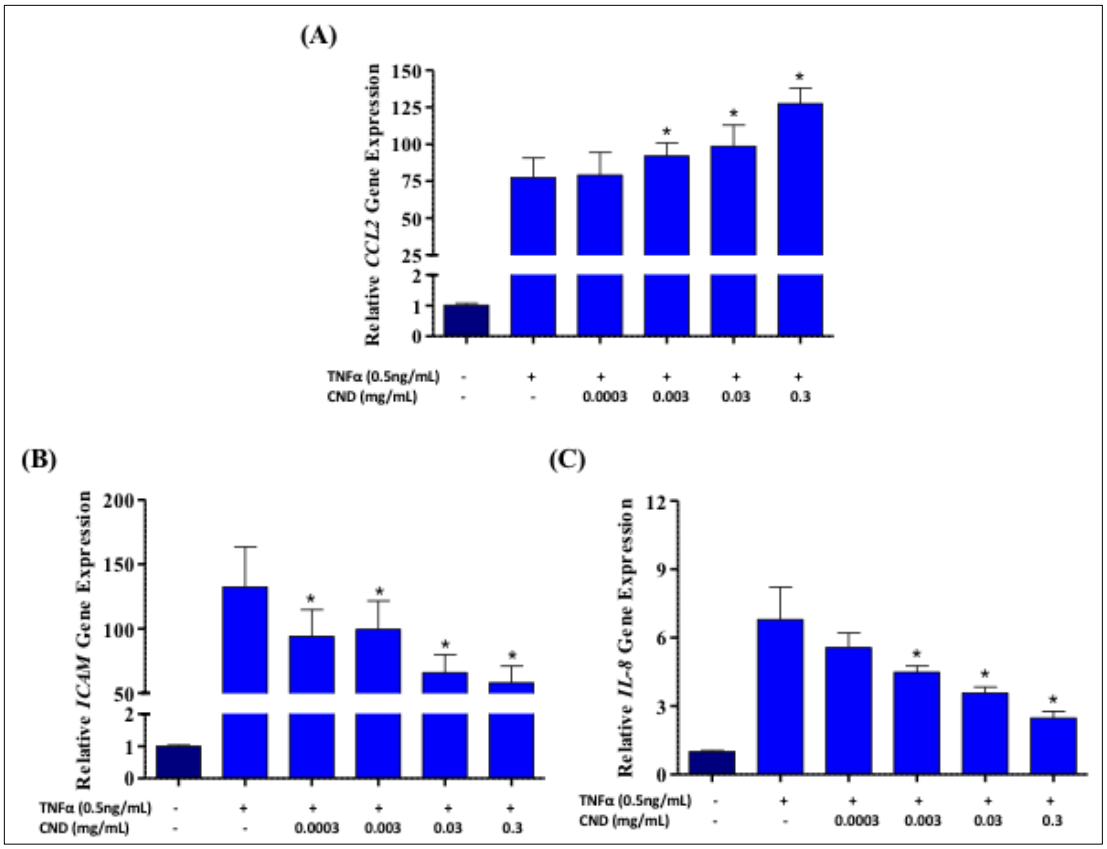

Figure 7. Effects of CNDs on TNF-α-Induced Expression of Pro-Inflammatory Genes. *EA.hy926 cells were co-treated for 24 hours with various concentrations of carbon nanodots and 0.5 ng/mL TNF-α. Gene expression was normalized using GAPDH as the house keeping gene.* ***(A) Gene expression of CCL2 genes induced by co-treatments.*** *The data shows that the target gene is upregulated after co-treatment.* ***(B) Gene expression of ICAM genes induced by co-treatments.*** *Our data shows a gradual decrease in the target gene expression after co-treatments.* ***(C) Gene expression of IL-8 genes induced by co-treatments.*** *The data shown shows a decrease in expression with increasing CND concentration co-treatments (data are in mean ± SEM, n=9, T-test data analysis, *p<0.05 vs. TNF-α).*

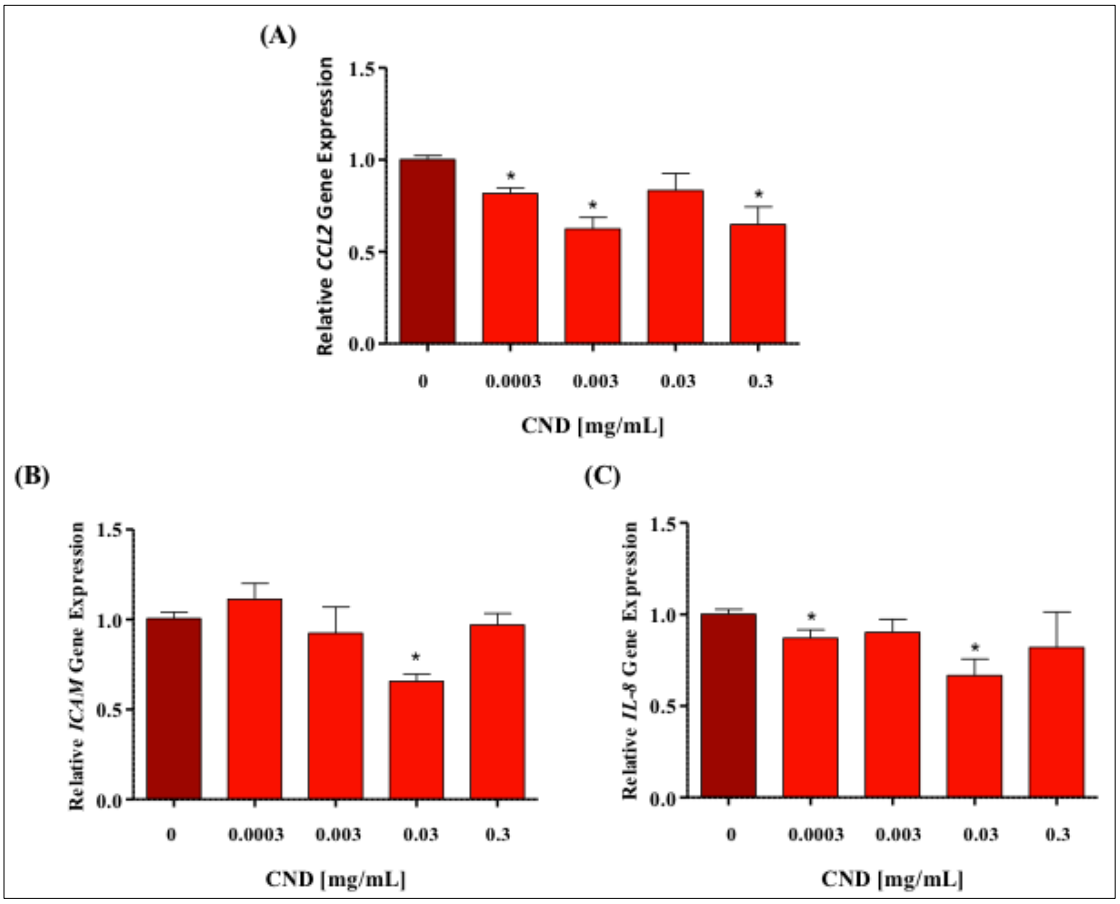

Figure 8. CNDs Affect the Expressions of Pro-Inflammatory Genes. *Cells were treated for 24hours various concentrations of carbon nanodots. mRNA levels were measured using qRT-PCR, Ct values were normalized to GAPDH expression. (A) MCP-1/CCL2 is a chemokine that recruits WBCS to the site of cellular damage. (B) ICAM/CD54 is a protein on endothelial cell surfaces that bind EC receptors for adhesion. , (C) IL-8 is a cytokine that causes WBC migration to the site of inflammation are pro-inflammatory genes of interest (data are in mean ± SEM, n=9, T-test data analysis, *p<0.05 vs. control).*

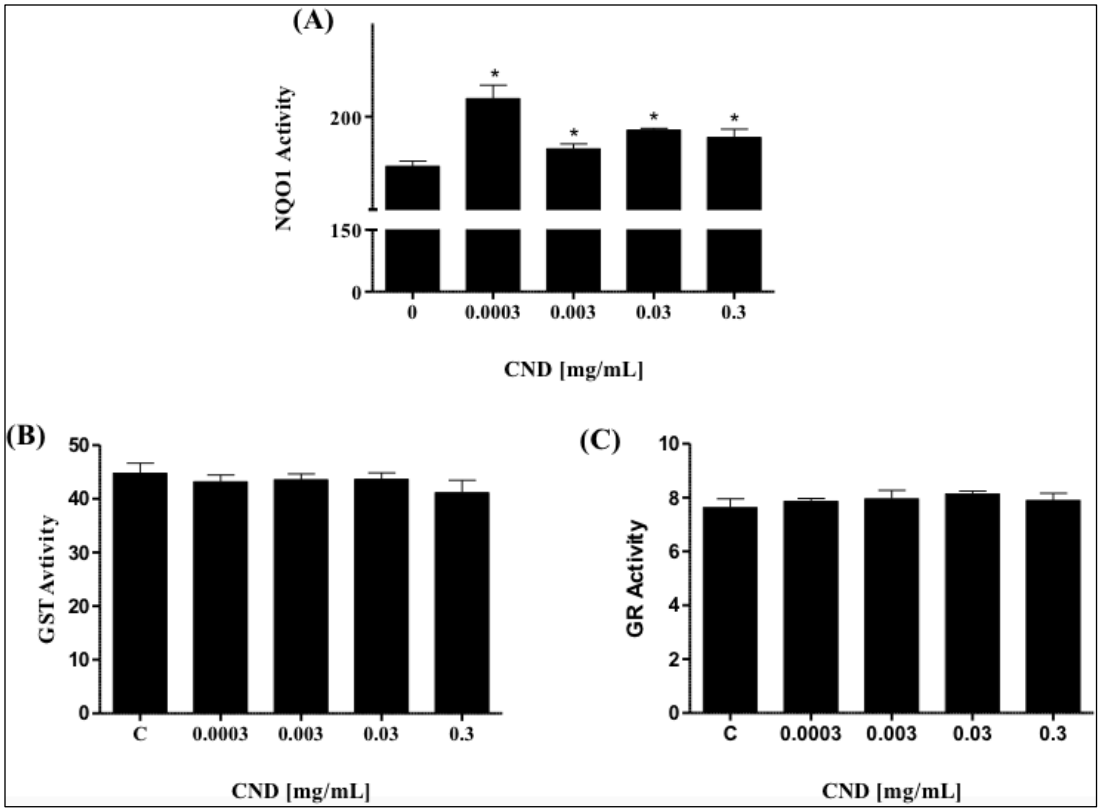

Figure 9. Increase in NOQ1 Activity by CNDs After 24 hr. *Antioxidant lysates were produced after CND exposure for 24 hrs in HBSS media. (A) NQO1 is an enzyme that scavenges for ROS; total activity was measured, when compared to the control 0.0003 mg/mL and 0.03 mg/mL CND were statistically significant. (B) The quantified GST activity for the conditions is not statistically significant compared to the control. (C) GR activity in the treatments is similar to the control, GR reduces GSSG to GSH, an important phase II enzyme. Data are in mean ± SEM (n=3), T-test data analysis*p<0.05 vs. control.*

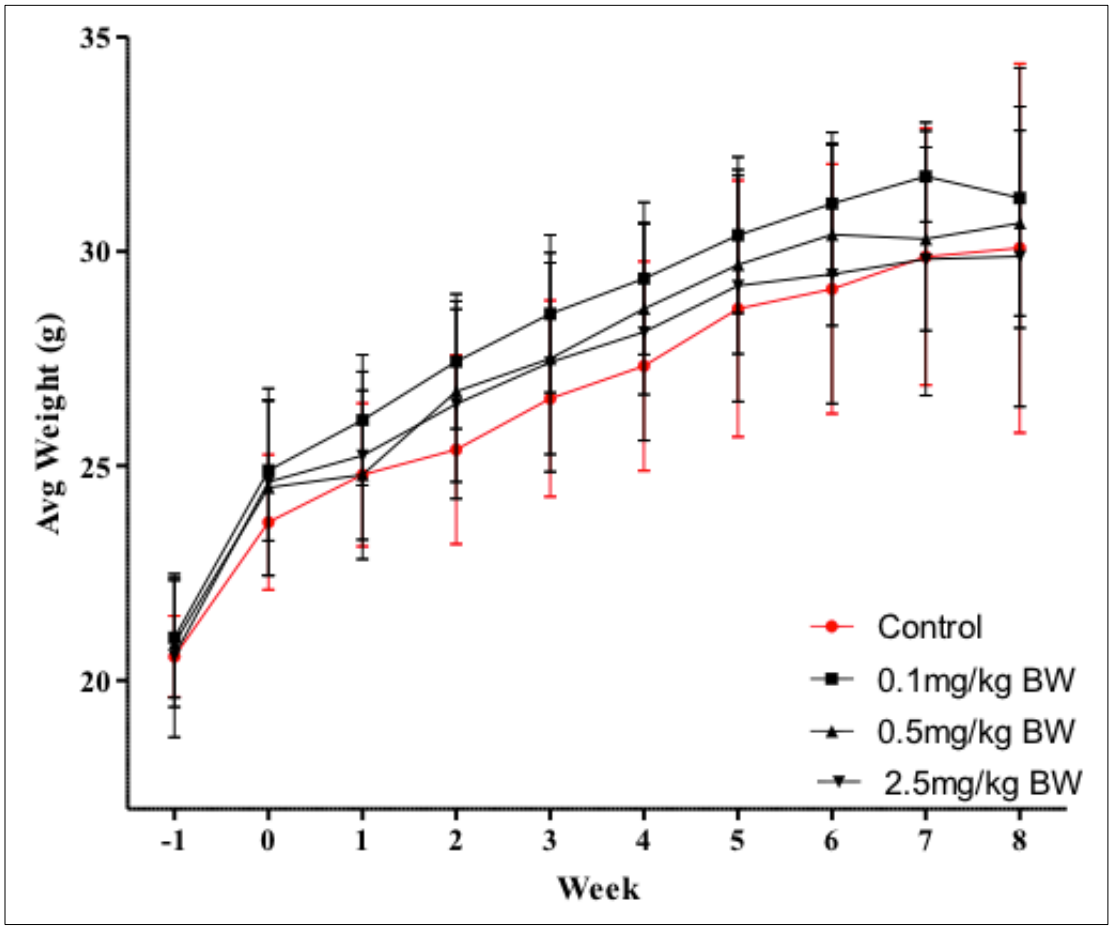

Figure 10. Average Weekly Body Weight of Apo E -/- Mice Dosed With CNDs Was Not Affected *. Animal models were fed an atherogenic diet one week prior to dosing, before starting the diet, animals were weighted (week -1), average body weight was collected weekly. No statistical significance was found when experimental groups were compared to the control of that week. All data represent mean ± SEM (n=6), 1-Way ANOVA analysis.*

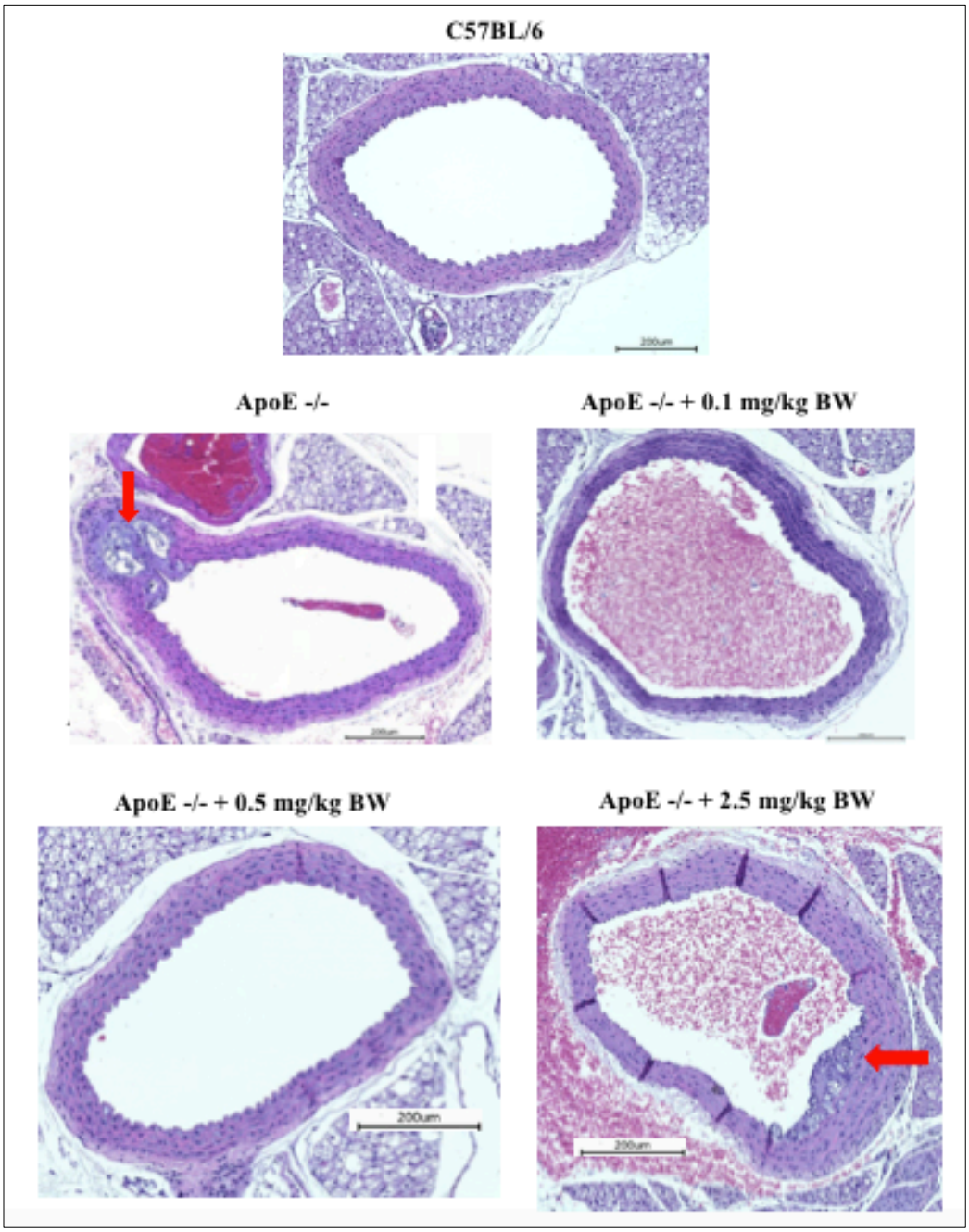

Figure 11. Histology of Aorta in ApoE -/- Mice Dosed with CNDs Suggests a Decrease in Plaque Formation. *ApoE -/- mice were dosed with carious concentrations of CNDs for 8 weeks via intraperitoneal dosing. Mice aorta samples were processed for hematoxylin and eosin staining. Top row left to right: C57 mice, ApoE -/-, ApoE -/- dosed with 0.1 mg/mL CND dosing; bottom row left to right: 0.5 mg/mL, 2.5 mg/mL CND dosing. Arrows indicate abnormal aorta structures. Keyence microscope was used for bright field microscopy; samples were sectioned at 5 microns.*

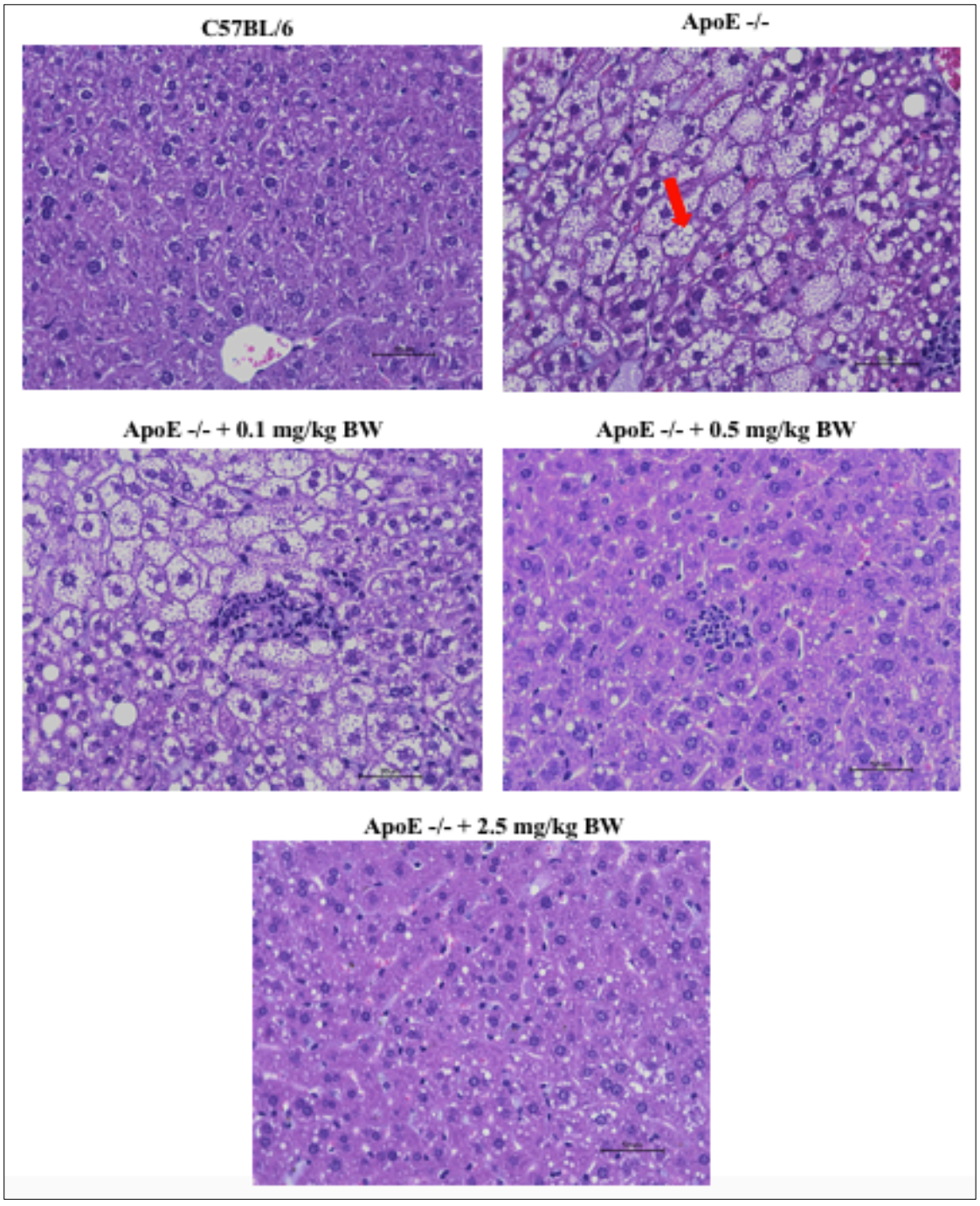

Figure 12. CNDs May Affect Hepatic Lipidosis in Apo E Deficient Mice. *Liver samples were processed and stained. Apo E -/- shows hepatic lipidosis due to apolipoprotein E deficiency. Histology imaging suggests that there seems to be a decrease in the accumulation of lipids in the liver with CND dosing. Arrow indicates hepatic lipidosis.*

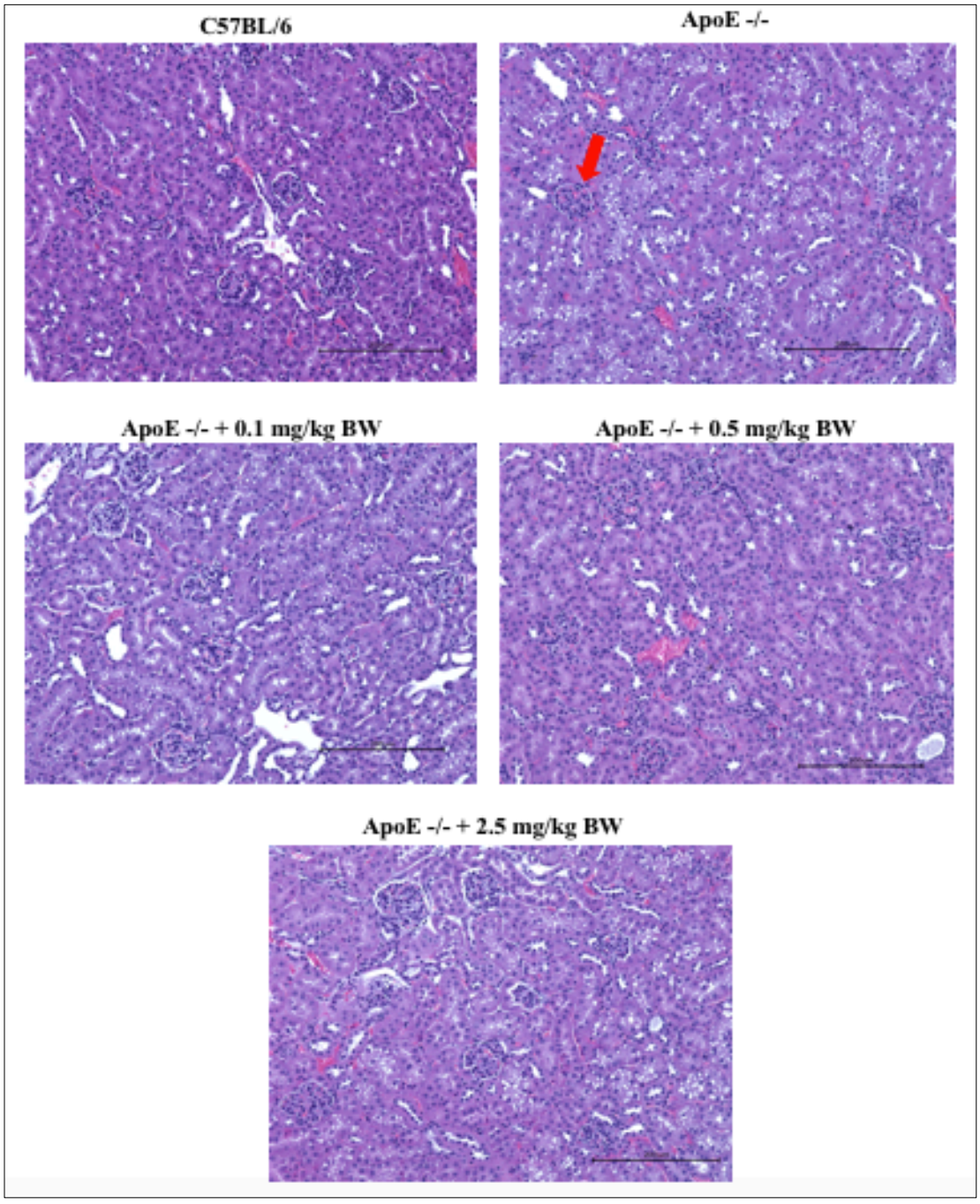

Figure 13. Carbon Nanodots Appear to Not Affect the Kidney. *Samples were processed for hematoxylin and eosin staining; imaging was done using Keyence microscope. Analysis of histology implies that carbon nanodots do not affect the kidney. Arrow indicates glomerulus.*

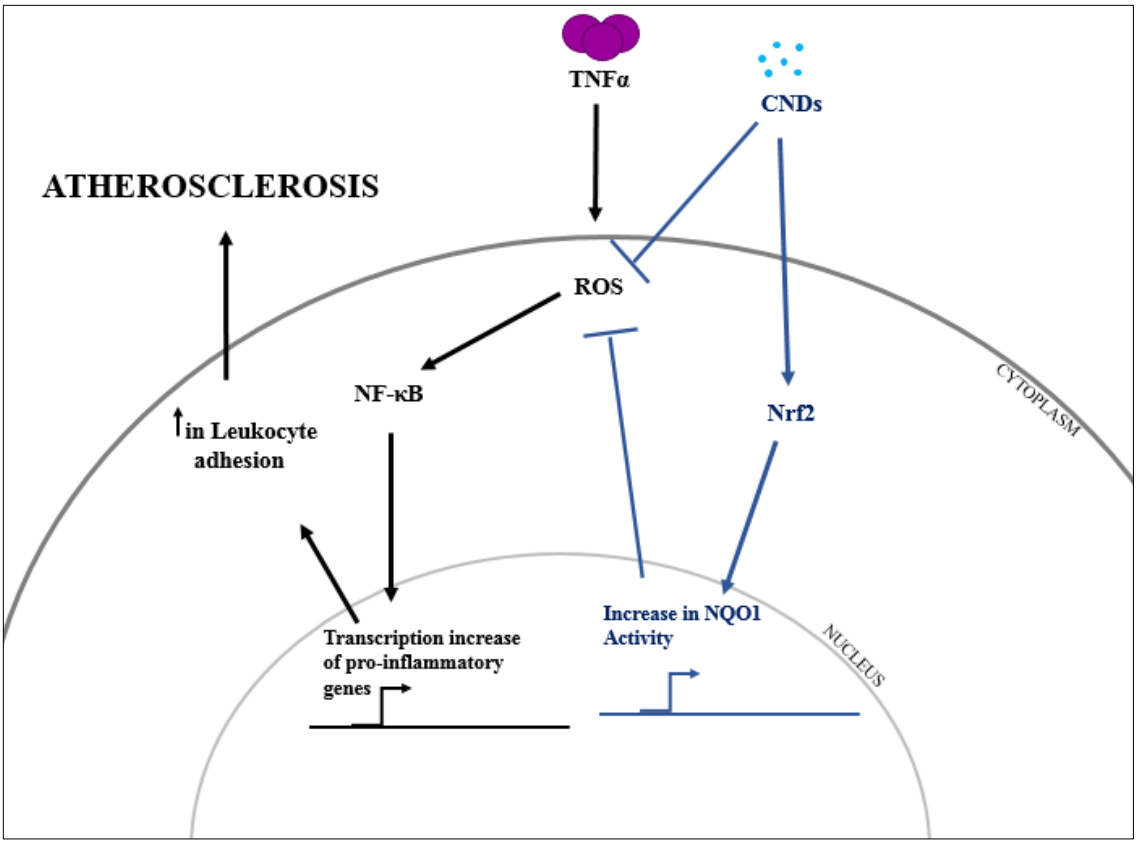

Figure 14. Diagram of Proposed Study: CND Modulation of TNF-α-Induced Endothelial Dysfunction